ADVANCED MATERIALS
www.advmat.de

The Road Towards Planar Microbatteries and Micro-Supercapacitors: From 2D to 3D Device Geometries

Shuanghao Zheng, Xiaoyu Shi, Pratteek Das, Zhong-Shuai Wu, and Xinhe Bao*

Dedicated to the 70th anniversary of Dalian Institute of Chemical Physics, CAS

The rapid development and further modularization of miniaturized and self-powered electronic systems have substantially stimulated the urgent demand for microscale electrochemical energy storage devices, e.g., microbatteries (MBs) and micro-supercapacitors (MSCs). Recently, planar MBs and MSCs, composed of isolated thin-film microelectrodes with extremely short ionic diffusion path and free of separator on a single substrate, have become particularly attractive because they can be directly integrated with microelectronic devices on the same side of one single substrate to act as a standalone microsized power source or complement miniaturized energy-harvesting units. The development of and recent advances in planar MBs and MSCs from the fundamentals and design principle to the fabrication methods of 2D and 3D planar microdevices in both in-plane and stacked geometries are highlighted. Additonally, a comprehensive analysis of the primary aspects that eventually affect the performance metrics of microscale energy storage devices, such as electrode materials, electrolyte, device architecture, and microfabrication techniques are presented. The technical challenges and prospective solutions for high-energy-density planar MBs and MSCs with multifunctionalities are proposed.

1. Introduction

The relentless development and integration of microscale electronics, such as micro-electromechanical systems, microrobots, implantable medical sensors, radio-frequency identification tags, remote environmental sensors, portable and wearable electronics, and their wireless self-powered micro/nanosystems, have greatly accelerated the ever-increasing need for microscale electrochemical energy storage systems.[1–6] Currently, microbatteries (MBs) and micro-supercapacitors (MSCs) are two representative microscale electrochemical energy storage devices,[7–9] which can be manufactured on the micro/nanoscale to be directly coupled with microelectronics[10–12] as standalone microscale power sources or complement miniaturized energy harvesters, such as solar cells[13,14] and nanogenerators,[15,16] mitigating the discontinuity, periodicity, and indeterminacy of renewable solar and mechanical energy. Such unitized microscale power sources or self-powered integrated microsystems are being deemed as necessary requirements for environmental, health, medical, industrial monitoring, and military applications.[17–22] Notably, most microelectronics can be normally operated with low power, ranging from nanowatts to milliwatts,[23–25] while with continuous boom of microelectronics high specific energy (per area or volume) of MBs and MSCs is being given top priority to run them for extended periods of time.[26–28] Furthermore, future microelectronics are projected to be miniaturized, flexible, aesthetic, smart, versatile, and integrable in form factors, and the same is expected for the MBs and MSCs.[29,30]

The nomenclature about what size of electrochemical energy storage device (e.g., MBs and MSCs) is able to be regarded as miniaturization still lacks a clear definition. In general, the devices referred to as MBs and MSCs represent a total footprint area in the square millimeter or even the square centimeter scale, and electrode thickness of less than 10 μm or arrays of separator-free microelectrodes with microscale size in at least two dimensions, or devices with 3D architectures on the scale of 1–10 mm^3 including all the components and associated packaging.[7,24,25,31] It is noted that this definition is also suitable for some unconventional energy storage devices, based on materials such as fiber, paper, and freestanding thin-film electrodes.[32–35] In this progress report, the planar MBs and MSCs refer to the system of two symmetric or asymmetric (anode vs cathode, or negative electrode vs positive electrode) dimensionally defined microelectrodes with in-plane or stacked geometry

S. H. Zheng, X. Y. Shi, P. Das, Prof. Z.-S. Wu, Prof. X. H. Bao
Dalian National Laboratory for Clean Energy
Dalian Institute of Chemical Physics
Chinese Academy of Sciences
457 Zhongshan Road, Dalian 116023, China
E-mail: wuzs@dicp.ac.cn
S. H. Zheng, X. Y. Shi, Prof. X. H. Bao
State Key Laboratory of Catalysis
Dalian Institute of Chemical Physics
Chinese Academy of Sciences
457 Zhongshan Road, Dalian 116023, China
S. H. Zheng, P. Das
University of Chinese Academy of Sciences
19 A Yuquan Rd, Shijingshan District, Beijing 100039, China
X. Y. Shi
Department of Chemical Physics
University of Science and Technology of China
96 Jinzhai Road, Hefei 230026, China

The ORCID identification number(s) for the author(s) of this article can be found under https://doi.org/10.1002/adma.201900583.

DOI: 10.1002/adma.201900583

built on one single substrate. Importantly, both of them can be directly coupled with integrated circuits on a microelectronic chip with desired compatibility.

As we know, MBs and MSCs possess quite different energy storage mechanisms. In general, MBs through reversible slow redox (insertion-type, conversion-type, and alloy-type) reaction deliver low self-discharge rate and high energy density (20–200 mWh cm^{-3}, 0.01–1 W cm^{-3}),[36–38] whereas MSCs can reversibly absorb and desorb electrolyte ions with a faster rate or undergo rapid Faradaic reaction at the interface between electrolyte and electrodes, endowing superior power density (10–1000 W cm^{-3}, 0.01–10 mWh cm^{-3}).[39–42] MBs, especially working in conventional liquid electrolyte, are restricted by low power density and short cycle life (normally <1000 times), which is not ideal for biomedical in vivo microsystems. Unlike MBs, MSCs are able to fully store energy in seconds or even in milliseconds, with the intriguing characteristics of free maintenance and long lifespan. Conventionally, commercial stacked batteries and supercapacitors are fabricated by sandwiching a porous polymer membrane as separator between two electrodes, consisting of active materials, conductive additives and binders, from slurry casted on metal based current collector (e.g., Cu, Al). As a result, the conventional stacked batteries and supercapacitors are too large and rigid,[43,44] making them hard to downscale their size to gain the miniaturization necessary for integration with microsystems. Therefore, innovative device geometries and unconventional microfabrication technologies of both MBs and MSCs with high performance metrics are being exploited for the miniaturization and integration of microelectronics.

2. Micro-Electrochemical Energy Storage Devices

In terms of the current trend in this field, we classified the planar micro-electrochemical energy storage devices (MEESDs) of MBs and MSCs into four types, including 2D stacked microdevices, 2D in-plane microdevices, 3D in-plane microdevices, and 3D stacked microdevices, based on the patterns and orientations of microelectrodes on one single substrate. As displayed in **Figure 1**, 2D stacked microdevices are typically made up of the multiply stacked layers starting with the bottom current collector, followed by anode, electrolyte, cathode, and top current collector in a vertical direction to the substrate through layer-by-layer deposition (Figure 1a). 2D in-plane microdevices, typically with interdigital geometry, are composed of two neighboring electrodes (anode and cathode) separated by micrometer interspaces in parallel arrangement on one side of the substrate (Figure 1b). 3D in-plane microdevices are constructed by vertically aligned isolated perpendicular pillar microelectrodes of interdigital anodes and cathodes on current collectors/substrate (Figure 1c), while 3D stacked microdevices are configured with conformal stacked layers of all the components (current collector, electrode, electrolyte) on 3D vertically aligned microstructured or nanostructured substrate (Figure 1d). It should be noted that, in a stacked architecture, the ions have to diffuse vertically throughout the thickness of the total microdevice, whereas in interdigitated configuration they move parallel to the substrate. The difference of ion diffusion leads to a slightly different electrochemical behavior in the stacked microdevices in comparison to the in-plane ones. Further, 2D stacked structure can make full use of the substrate footprint area, while the microelectrode area in the 2D in-plane configuration was reduced by at least a factor of 2, caused by the interspaces between two neighboring microelectrodes. As a result, the areal

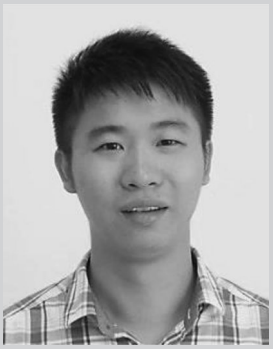

Shuanghao Zheng is pursuing a Ph.D. degree from Dalian National Laboratory for Clean Energy, Dalian Institute of Chemical Physics (DICP), Chinese Academy of Sciences (CAS), under the supervision of Prof. Xinhe Bao and Prof. Zhong-Shuai Wu. He obtained his B.S. degree in applied chemistry from Changsha University of Science & Technology in 2014. His research interests focus on graphene and 2D materials and miniaturized energy storage devices.

Zhong-Shuai Wu received his Ph.D. in materials science from the Institute of Metal Research, CAS in 2011, and worked as a postdoc at the Max-Planck Institute for Polymer Research, Mainz, Germany, in 2011–2015. He then joined DICP as a full professor and group leader of 2D Materials & Energy Devices. His research focuses on graphene and 2D materials, supercapacitors, micro-supercapacitors, batteries (Li–S/metal, Li-, Na-, K-, Zn-, Al-ion), microbatteries, flexible and planar energy-storage devices.

Xinhe Bao received his Ph.D. in physical chemistry from Fudan University in 1987. He held an Alexander von Humboldt Research Fellow position in Fritz-Haber Institute, Berlin, Germany, between 1989 and 1995, hosted by Prof. Gerhard Ertl. Following that, he joined DICP as a full professor. He became a member of the CAS in 2009. His research interest is nano and interfacial catalysis, focusing on the fundamental understanding of heterogeneous catalysis, including development of new catalysts and novel catalytic processes related to energy conversion and storage.

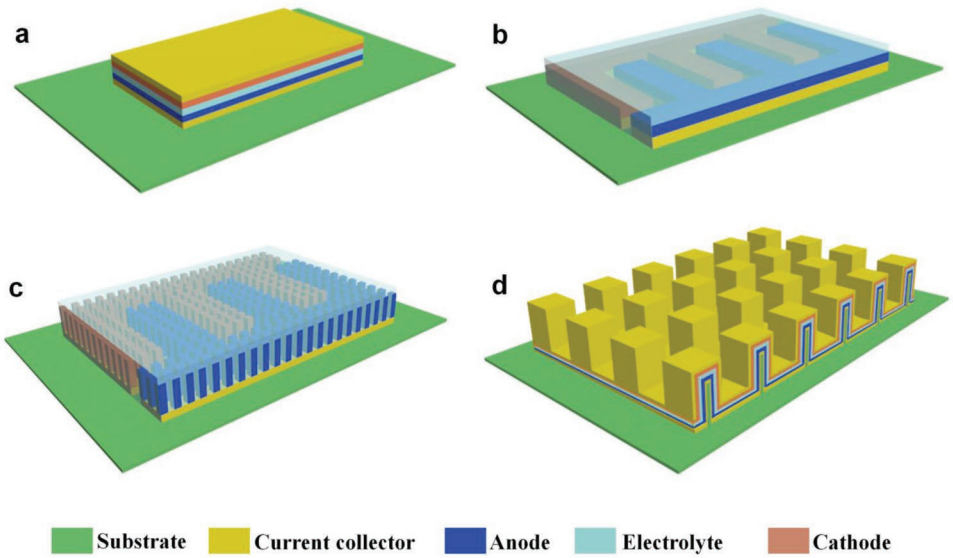

Figure 1. Schematic of the classified four types of MEESDs. a) 2D stacked microdevice. b) 2D in-plane microdevice. c) 3D in-plane microdevice. d) 3D stacked microdevice.

capacity or capacitance of 2D stacked microdevices is twice more than that of 2D in-plane ones at the same thick microelectrodes in principle.

The 3D MEESDs developed are to highly increase the mass loading of active materials, provide a comparable areal normalized performance closed to those of bulky devices, and simultaneously maintain their structural superiority of 3D microelectrodes for high power performance. In the case of 3D stacked architecture, the formation of 3D structural microelectrodes mainly relies on the 3D supporting substrate. The full containment of anode, cathode, and electrolyte/separator as well as supporting substrate truly leads to less than one half effective space for anode or cathode. Therefore, 3D in-plane and stacked microdevices basically have similar areal performance for the same thick electrodes. It is worth noting that both 2D and 3D stacked MEESDs require gel-like or solid electrolyte as separator to avoid short circuit, while in-plane MEESDs are free of separators, and can be well operated in both liquid-state and solid-state electrolytes. Since the thin solid-state electrolyte (also acting as separator) is sandwiched between anode and cathode, the stacked MEESDs hold unique performance metrics in developing arbitrary-shaped on-chip devices, which could not be achieved in the interdigitated counterparts because their anodic and cathodic microelectrodes cannot intersect each other.[45,46] Consequently, this unique arbitrary-shape feature for stacked microdevices enables them to fully couple with the residual space in integrated circuits, enhance the aesthetic versatility, and miniaturize the array dimensions of power source-integrated electronics.

3. Microbatteries

MBs have been developed for at least 30 years, and possess an intrinsic virtue of high energy density. However, they are primarily limited by short lifetime and poor power density due to the slow ion intercalation charge-storage mechanism and low ionic conductivity of solid-state electrolyte. As illustrated in **Figure 2**, the timeline briefly introduces the development process of planar MBs from 2D to 3D configuration, and from stacked to in-plane geometry, including nanostructured materials, innovative device configurations, battery types, and microfabrication technologies. And various MBs with representative areal and volumetric performance metrics are summarized in **Table 1**.

3.1. 2D Stacked MBs

The 2D stacked MBs, also named as thin-film MBs, were first developed among the four-types of MBs in 1983,[57] mainly referring to thin-film lithium ion MBs. Kanehori et al.[57] first reported the fabrication of thin-film lithium ion MBs using TiS_2 as cathode, glassy solid electrolyte of $Li_{3.6}Si_{0.6}P_{0.4}O_4$, and metallic lithium as anode through chemical vapor deposition (CVD) and magnetron sputtering. These binder-free and additive-free MBs exhibited excellent cycling stability up to 2000 times because of short Li-ion transport pathway. Subsequently, various electrode and electrolyte materials have been exploited for 2D stacked MBs. Typically, i) the positive electrodes include metal oxides (V_2O_5),[65] lithium transition metal layered oxides (marked as LMO, such as $LiCoO_2$,[66] $LiMn_2O_4$[67]), olivine and polyanion compounds ($LiFePO_4$),[68] and doped LMO-like materials ($LiNiCoO_2$).[69] ii) The negative electrodes cover carbon-based materials (graphite[70] and porous carbon[71]), silicon,[72,73] lithium,[59] and Ti compounds (TiO_2[74] and $Li_4Ti_5O_{12}$[75]). iii) Solid-state electrolytes involve ion-conductive $LiNbO_3$–SiO_2,[76] Li_2S–P_2S_5,[77] lithium lanthanum titanium oxides ($Li_{3x}La_{(2/3)-x}TiO_3$),[78] glassy amorphous lithium phosphates (Li_2O–P_2O_5–SiO_2),[79] lithium phosphorus oxynitride (LiPON),[80] $Li_{14}Zn(GeO_4)_4$,[81] and polymers[82,83] as both electrolyte and separator. Most reported inorganic solid-state electrolytes have low ionic conductivity

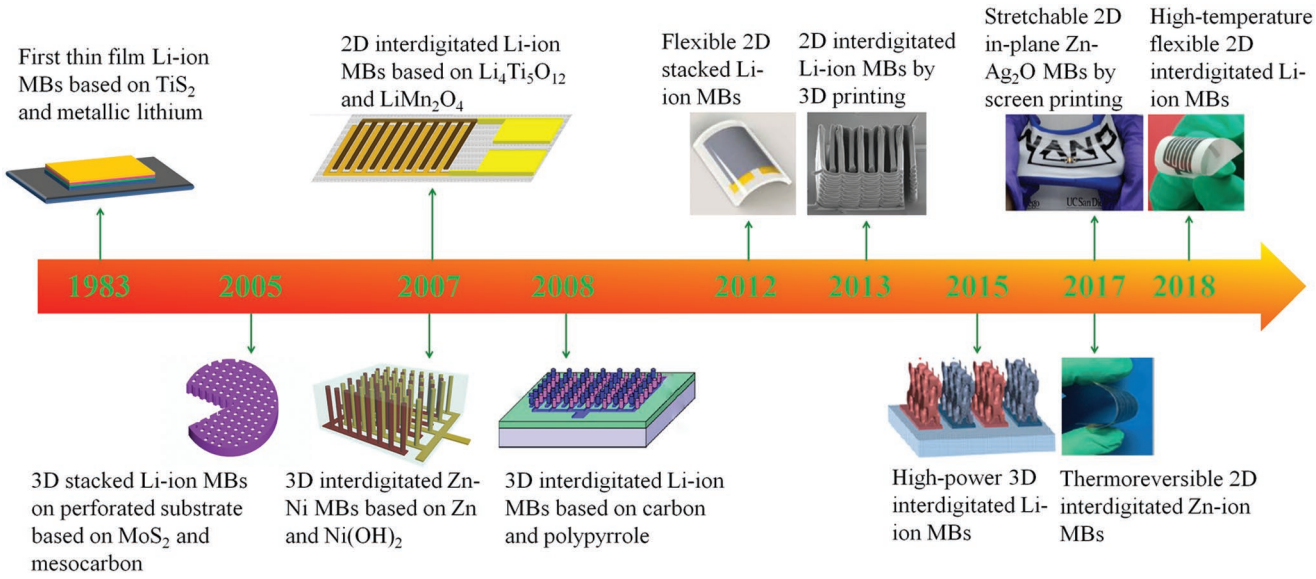

Figure 2. A brief timeline of the development history of representative planar MBs. Inset images: "3D stacked Li-ion MBs on perforated substrate based on MoS_2 and mesocarbon,"[47] "2D interdigitated Li-ion MBs based on $Li_4Ti_5O_{12}$ and $LiMn_2O_4$". Reproduced with permission.[48] Copyright 2007, Elsevier. "3D interdigitated Zn-Ni MBs based on Zn and $Ni(OH)_2$."[49] "3D interdigitated Li-ion MBs based on carbon and polypyrrole." Reproduced with permission.[50] Copyright 2008, Elsevier. "Flexible 2D stacked Li-ion MBs." Reproduced with permission.[51] Copyright 2012, American Chemical Society. "2D interdigitated Li-ion MBs by 3D printing." Reproduced with permission.[52] Copyright 2013, Wiley-VCH. "High-power 3D interdigitated Li-ion MBs." Reproduced with permission.[53] Copyright 2015, National Academy of Sciences. "Stretchable 2D in-plane Zn-Ag_2O MBs by screen printing." Reproduced with permission.[54] Copyright 2017, Wiley-VCH. "Thermoreversible 2D interdigitated Zn-ion MBs." Reproduced with permission.[55] Copyright 2017, Wiley-VCH. "High-temperature flexible 2D interdigitated Li-ion MBs." Reproduced with permission.[56] Copyright 2018, Elsevier.

of about 10^{-5} S cm^{-1}, while polymer-based electrolytes usually achieve higher ionic conductivity at the level of 10^{-3} S cm^{-1} at room temperature, which are hardly comparable with the commercial organic liquid electrolyte (10^{-2} S cm^{-1}). Additionally, a variety of thin-film micromechanical techniques, such as CVD,[84] physical vapor deposition,[85] thermal evaporation,[51] magnetron sputtering,[86,87] sol–gel solution,[88,89] and atomic layer deposition (ALD),[90] have been proposed for the fabrication of these thin-film MBs. However, most stacked lithium ion MBs suffer from low power density and poor rate capability due to low electrical conductivity of electrode films and inferior ionic conductivity of solid-state electrolyte, therefore, new solid-state electrolytes with high ionic conductivity need to be explored urgently. To meet the stringent requirement of flexible, miniaturized devices, it is crucial to design thin-film MBs with superior mechanical stability for direct integration with flexible electronics. For instance, Lee and co-workers[51] developed a bendable thin-film battery with a sandwich structure of $LiCoO_2$, LiPON, and metallic lithium, fabricated via magnetron sputtering and thermal evaporation and followed by a universal transfer approach through sticky tapes (**Figure 3**a–d). The resultant MBs showed excellent flexibility without capacity fade at serious deformation and with slight voltage decay under repeated bending tests for 20 000 times. Such device delivered considerable energy density of 2.2 mWh cm^{-3} with a large discharged plateau of 3.9 V. Moreover, this microdevice can be seamlessly integrated with an organic light-emitting diode (LED) to form an all-in-one flexible display system. Subsequently, the flexible MBs based on Li/lithium boron oxynitride (LiBON)/$LiCoO_2$ were constructed through sophisticated fabrication techniques like magnetron sputtering, thermal evaporation, and in situ encapsulation.[59] The protective encapsulation consisted of polyacrylate film by ultraviolet (UV) polymerization and aluminum oxide layer. It is worth noting that the total thickness of the full device is only 10 µm including the encapsulated layer. As a result, the as-fabricated MBs displayed high volumetric discharge capacity of 49.2 µAh cm^{-2} $µm^{-1}$ (based on cathode layer), excellent capacity retention of 90% after 1000 cycles, and remarkable mechanical integrity under severe bending and twisting states. Notably, the MBs could be operated at a wide temperature range from −10 to 60 °C and delivered high rate capability up to 30 C at 20 °C. It is suggestive that such microdevices provide diverse opportunities for future flexible and wearable miniaturized electronics.

The solid-state electrolytes for MBs have the intrinsic advantages of nonflammability, nonvolatility, no leakage of liquid electrolytes, outstanding shape compatibility, and improved safety. Nevertheless, the areal capacity of such 2D stacked MBs is still very limited due to the thinness of electrode film, usually <5 µm. By increasing the thickness of film electrodes, higher areal capacity could be achieved. But the thick electrode films would produce longer diffusion distance for electrolyte ions and decrease electrical conductivity of electrode. If the whole mixed ion-electron conductive network of electrode is not appropriately built, the volumetric capacity, rate capability, and power density of MBs will be dramatically reduced. Moreover, the rigid and thick electrode films could be harmful for the construction of flexible 2D stacked MBs induced by the weakened interfaces and integrity of stacked films on the substrate during repeated mechanical deformation. In addition,

Table 1. Summary of the electrochemical performance of different planar MBs. *V*: Voltage. C_A: Areal capacity. C_V: Volumetric capacity. E_A: Areal energy density. P_A: Areal power density. E_V: Volumetric energy density. P_V: Volumetric power density. EC: Ethylene carbonate. DEC: Diethyl carbonate. PMMA: Polymethyl methacrylate. DMC: Dimethyl carbonate. P_{14}TFSI: 1-butyl-1-methyl-pyrrolidinium bis(trifluoromethylsulfonyl) imide. PVDF-HFP: Poly(vinylidene difluoride-co-hexafluoro-propylene). PC: Propylene carbonate. PPy: Polypyrrole.

Types	Electrodes	Thickness [μm]	Electrolyte	V	C_A [μAh cm^{-2}]	C_V [mAh cm^{-3}]	E_A [μWh cm^{-2}]	P_A [mW cm^{-2}]	E_V [mWh cm^{-3}]	P_V [W cm^{-3}]	Stability	Refs.
2D stacked MBs	Li//LiS_2	4//3.7	$Li_{3.6}Si_{0.6}P_{0.4}O_4$	1.5–2.5	150[a]	–	300[c]	–	–	–	2000 (75%)	[57]
	Li//$LiCoO_2$	–//0.1	$Li_{0.5}La_{0.5}TiO_3$	3.3–4.3	–	5[b]	–	–	19[c]	–	300 (65%)	[58]
	Li//$LiCoO_2$	3//5	LiPON	3–4.2	106[a]	–	413[c]	–	2[a]	–	100 (99%)	[51]
	Li//$LiCoO_2$	1//1.7	LiBON	3–4.2	29[c]	–	113[a]	–	83.6[c]	–	1000 (90%)	[59]
2D in-plane MBs	$Li_4Ti_5O_{12}$//$LiMn_2O_4$	0.6//1	1 M $LiClO_4$/EC/DEC/PMMA	1.5–3	4.5[a]	–	11[c]	–	–	–	–	[48]
	$Li_4Ti_5O_{12}$//$LiCoO_2$	15//15	1 M $LiClO_4$/EC/DEC/PMMA	1.5–2.5	270[b]	–	670[c]	–	–	–	–	[60]
	Ni–Sn//Li_x MnO_2	15//15	1 M $LiClO_4$/EC/DEC	2–4	–	–	225[c]	11[c]	150[a]	74[a]	15 (64%)	[61]
	$Li_4Ti_5O_{12}$//$LiFePO_4$	150//150	1 M $LiClO_4$/EC/DMC	1–2.5	1200[b]	–	2700[b]	20[b]	–	–	30 (96%)	[52]
	$Li_4Ti_5O_{12}$-EG// $LiFePO_4$-EG	5//7	LiTFSI/P_{14}TFSI/PVDF-HFP	1–2.4	40[c]	67.7[b]	75[b]	5[b]	125[b]	8.8[b]	3300 (100%)	[56]
	Zn//MnO_2	530//530	6 M KOH	1–1.5	3800[b]	–	4700[b]	–	–	–	–	[62]
3D in-plane MBs	Ni–Sn//Li_x MnO2	10//10	1 M $LiClO_4$/EC/DEC	1.4–3.2	23[c]	23[a]	65[c]	36[c]	65[a]	36[a]	100 (80%)	[53]
	Carbon//PPy	62//65	1 M $LiClO_4$/EC/DMC	0.7–3.5	10[a]	10[c]	20[c]	–	20[c]	–	–	[50]
	Zn//$Ni(OH)_2$	400//400	6 M KOH	1.3–1.7	2.5[a]	–	4.3[a]	–	–	–	–	[49]
3D stacked MBs	Mesocarbon//MoS_2	500//500	1 M $LiPF_6$/EC/DEC	1.3–2.2	2000[a]	40[c]	3500[c]	–	70[c]	–	200 (60%)	[47]
	Lithiated Si// $LiNi_{0.8}Co_{0.15}Al_{0.05}O_2$	400//400	1 M $LiClO_4$/PC/SU-8 Photoresist	2.2–3.7	1800[a]	90[c]	5200[a]	–	260[a]	–	100 (92%)	[63]
	Li//TiO_2	–//78	1 M LiTFSI/EC/DEC	1.1–2.3	370[b]	–	–	–	–	–	40 (100%)	[64]

[a]Reported values based on footprint area or volume of device; [b]Reported values based on electrode area or volume. The thickness referred to the whole anode and cathode; [c]Calculated values according to the reported literatures.

most 2D stacked MBs reported previously are related to solid-state inorganic electrolytes and polymer-based organic electrolytes, but aqueous based systems for such microdevices have not been well explored. Taking into consideration the high ionic conductivity, safety issue, environmental friendliness, and biological compatibility, developing aqueous based thin-film MBs, in particular working in "water-in-salt" that can stably extend voltage to 3 V,[91] and coupling with high areal or volumetric energy density and superior rate performance, will be a competitive option for the portable and wearable electronics. Further, aqueous electrolyte with an immiscible fluorinated additive would efficiently form organic and inorganic fluorides based interphase and resolve cathodic stability limit to assemble high-voltage (4 V) aqueous lithium ion MBs with enhanced safety.[92]

3.2. 2D In-Plane MBs

2D in-plane MBs consist of parallel microelectrodes next to each other on single substrate operated at liquid or solid-state electrolyte. Such microdevices, free of separator, allow for fast and multidirectional diffusion of electrolyte ions due to in-plane geometry. In this case, high power density can be achieved by narrowing the width and optimizing structural design of patterned microelectrodes and decreasing the interspace width of the neighboring microelectrodes. Typically, Kanamura and co-workers[48,93] manufactured the electrode microarrays of $LiMn_2O_4$ and $Li_4Ti_5O_{12}$ on interdigital Au current collectors via microinjection technique. The resultant all-solid-state MBs with polymer gel electrolyte could be operated at high current density of 50 C and exhibited remarkable rate capability due to short interspace (50 μm) between microelectrodes and high ionic conductivity (1 mS cm^{-1}) of gel electrolyte. Afterward, King and co-workers[61] fabricated in-plane lithium ion MBs by direct electrodeposition of thin layer of nickel-tin as anode and lithiated manganese oxide as cathode on the interdigitated porous nickel scaffolds (Figure 3e,f). The resultant microdevices, dependent on the thickness of active materials used, delivered ultrahigh power density of 2.4–7.4 mW cm^{-2} μm^{-1} at ultrahigh current densities of 250–1000 C, at least two orders of magnitude higher than those of other MBs (0.1–5 C).[50,94] The exceptional performance of such microdevices was attributed to reasonable construction of both opposite microelectrodes with abundant nanoporous structure, and extremely small interspaces of 10 μm between adjacent microelectrode fingers, significantly

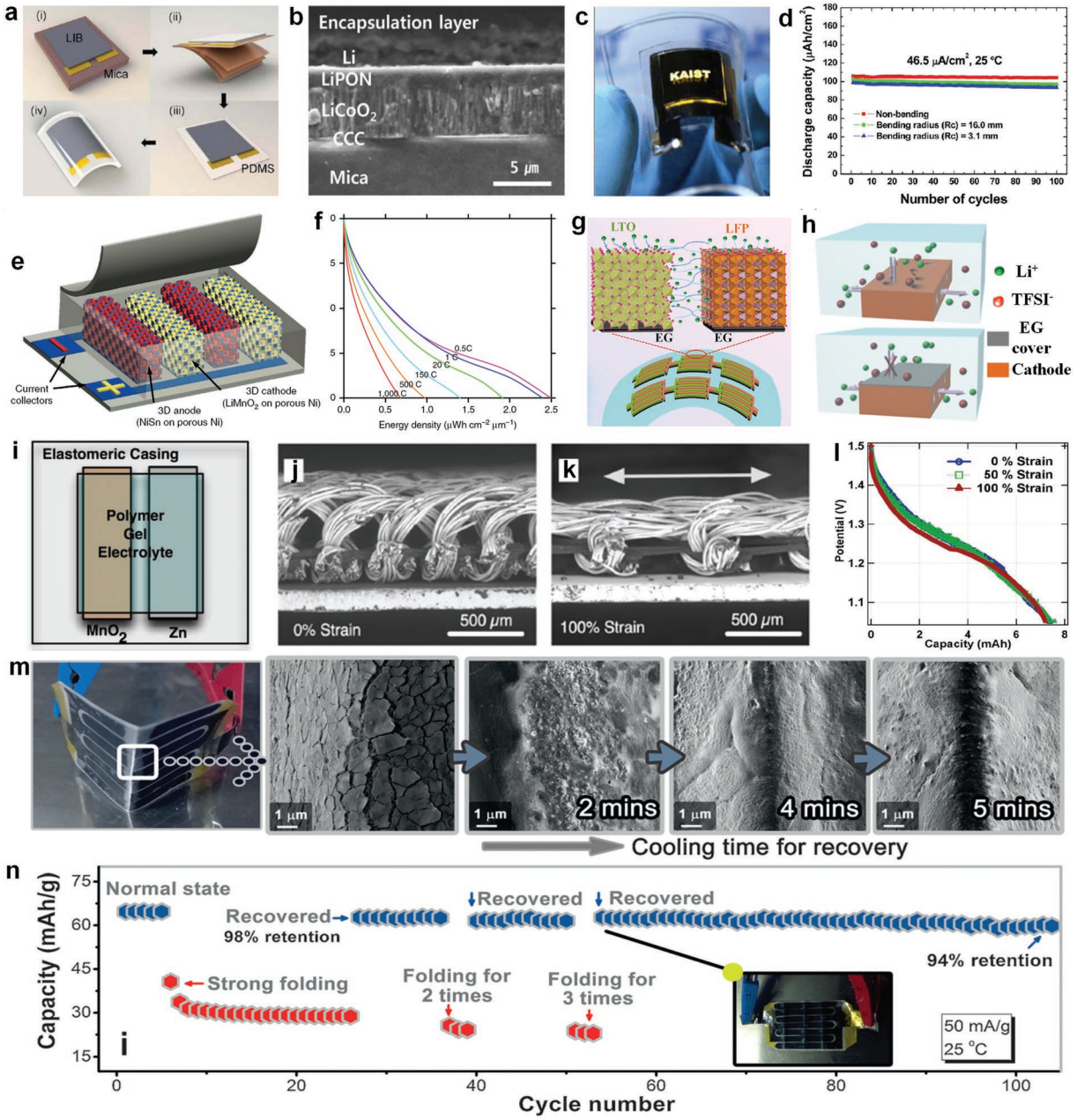

Figure 3. 2D stacked and in-plane MBs. a) Schematic of the fabrication of flexible 2D stacked lithium ion MBs. b) Cross-section SEM image of the stacked MBs. c) Photograph of an all-in-one flexible LED system integrated with the flexible stacked MBs. d) Capacity retention at different bending states. a–d) Reproduced with permission.[51] Copyright 2012, American Chemical Society. e) Schematic showing planar lithium ion MBs with interdigital patterns of anode and cathode on a nickel scaffold. f) Discharge curves at various current densities from 0.5 to 1000 C. e,f) Reproduced with permission.[61] Copyright 2013, Nature Publishing Group. g) Schematic of flexible integrated lithium ion MBs with multidirectional Li-ion diffusion mechanism. h) Schematic of ion transfer in microelectrodes without and with EG cover. g,h) Reproduced with permission.[56] Copyright 2018, Elsevier. i) Schematic of stretchable interdigital Zn-MnO_2 MBs. j,k) SEM images of the fabric under j) 0% to k) 100% strain. l) Discharge curves of Zn-MnO_2 MBs tested at 0%, 50%, and 100% strain. i–l) Reproduced with permission.[62] Copyright 2012, Wiley-VCH. m) SEM images of interdigital planar Zn-based MBs showing the broken area recovered after cooling for 2, 4, and 5 min at −5 °C. n) Cycling stability of Zn-based MBs with folding for 3 times. m,n) Reproduced with permission.[55] Copyright 2017, Wiley-VCH.

shortening lithium ion diffusion pathway. Very recently, our group developed a one-step mask-assisted device fabrication technique for facile construction of all-solid-state flexible lithium ion MBs with $Li_4Ti_5O_{12}$ nanospheres/electrochemically exfoliated graphene (EG) as anode and $LiFePO_4$ microspheres/EG as cathode on a nylon membrane, using ionogel electrolyte of bis(trifluoromethanesulfonyl)imide lithium salt (LiTFSI), 1-butyl-1-methylpyrrolidinium bis(trifluoromethanesulfonyl)imide (P_{14}TFSI), and poly(vinylidene difluoride-co- hexafluoropropylene) (PVDF-HFP) (LiTFSI/P_{14}TFSI/PVDF-HFP) (Figure 3g).[56] The

as-fabricated lithium ion MBs exhibited long-term cyclability with 100% of initial capacity retained up to 3300 cycles, exceptional flexibility without capacity fade under repeated serious bending and twisting, and high-temperature stability up to 100 °C. The outstanding electrochemical performances of these MBs are primarily ascribed to the full consideration of various components of batteries, including high-capacity electrode materials, screening stable electrolyte, electrode design, and strongly coupled interfaces. It is pointed out that, with a smooth EG layer covered on the top surface of microelectrodes, the as-obtained planar lithium ion MBs have proved to possess multidirectional lithium ion diffusion mechanism, in which electrolyte ions could transfer from two side surfaces and the top surface of microelectrodes (Figure 3h), resulting in dramatically enhanced rate capability. So far, only a few 2D in-plane lithium ion MBs have been constructed with smart functional flexibility, such as foldability, stretchability, and self-repairability. The major challenge lies in the inflexibility and nonstretchablity of electrode materials, e.g., graphite, metal oxides, $Li_4Ti_5O_{12}$, $LiFePO_4$, $LiCoO_2$, and $LiMn_2O_4$. To overcome this issue, these stiff materials are usually transferred into deformable composites combined with the inherently flexible and elastic supports, from nanocarbons (e.g., graphene, carbon nanotubes (CNTs), and carbon nanofiber) to conducting polymers (e.g., polyaniline, poly(3,4-ethylenedioxythiophene)).[37,43,95]

To realize scalable integration and applicability, several simple and scalable strategies, e.g., inkjet printing,[96,97] spray printing,[98] and screen printing,[99–101] have been proposed to manufacture microelectrodes or batteries on either flexible or inflexible substrates. In particular, along with the rapid development of new techniques, the novel scalable 3D printing microfabrication was initially used to fabricate 2D in-plane MBs. For example, Lewis and co-workers[52] reported the 3D printing fabrication of interdigitated lithium ion MBs without need for templates based on interdigital microelectrodes of $Li_4Ti_5O_{12}$ and $LiFePO_4$ on Au current collectors. The patterned microelectrodes could be precisely stacked through layer-by-layer deposition, thereby such microdevices presented high areal energy density of 9.7 J cm^{-2}. Hu and co-workers[102] fabricated all components 3D-printed lithium ion MBs, with interdigital electrodes free of metal current collectors, through 3D printing of hybrid microelectrodes and solid-state electrolyte inks. Graphene oxide (GO)-based composite inks comprising $Li_4Ti_5O_{12}$ or $LiFePO_4$ and highly concentrated GO solution were used to fabricate the lithium ion MB prototypes. After thermal annealing, the printed microelectrodes showed highly increased electrical conductivities of 31.6 S cm^{-1} for cathode and 6.1 S cm^{-1} for anode. The full cell delivered a discharge capacity of about 100 mAh g^{-1} with a notable cycling stability. The emerging and promising 3D technology for such patterned MBs can be further engineered with high precision to accurately control the finger thickness, finger width, and interspace of adjacent interdigital fingers. Furthermore, the extrusion-based inks should have high apparent viscosity, high ratio of active materials, and superior electrical conductivity after solidification. In addition, most reported 2D in-plane MBs have a small voltage window (≤3 V) that translates to the restriction of energy density due to the application of high potential (vs Li^+/Li) Ti-based materials as anode, rather than graphite and silicon. However, low lithiation potential (vs Li^+/Li) graphite and silicon as anode always encounter huge volume expansion that would remarkably degrade the contact interface between microelectrodes and current collectors or/and solid-state electrolyte, and eventually generate poor cycling performance. Therefore, the elaborated screening of high-capacity active materials and rational design of microelectrodes with nanoporous and conductive network that can intrinsically accommodate volume expansion through innovative manufacturing process is an effective way to assemble high areal or volumetric capacity MBs.

Beyond the abovementioned lithium ion MBs, 2D in-plane zinc-based MBs with various functions like flexibility, stretchability, and self-recovery have been developed. For instance, Steingart and co-workers[62] designed stretchable Zn-based MBs with active materials of Zn and MnO_2 embedded in a compliant conductive fabric with ultrahigh load of 16 and 12.8 mg cm^{-2}, respectively. The resultant stretchable Zn ion MBs showed a rather high areal capacity of 3.8 mAh cm^{-2}, and no degradation of capacity under strain as high as 100% (Figure 3i–l). Even though stretched up to 150% in horizontal direction and twisted by 90° in vertical direction, the MBs could still sufficiently work. Afterward, Cui and co-workers[55] explored the cooling-recovery flexible Zn-based MBs with interdigital pattern of Zn as anode and $LiFePO_4$ or $LiMn_2O_4$ as cathode, using thermoreversible polymer poly(ethylene oxide)-poly(propylene oxide)-poly(ethylene oxide) (PEO_{53}–PPO_{34}–PEO_{53}) gel electrolyte. When a mechanical damage occurred at the electrode–electrolyte interface, a simple cooling stimulation would rapidly repair and refresh the broken interface within 5 min of MBs providing a high healing efficiency of capacity up to 98% after being folded (Figure 3m and n). Further, a wearable charge system was constructed by integrating the flexible Zn-based MBs with a solar cell and thermocell, demonstrative of great potential integration with wearable microelectronics. In addition, all-solid-state flexible Zn ion MBs were constructed via direct electrodeposition of MnO_2 and Zn nanosheets on interdigital carbon nanotube films supported on thin polydimethylsiloxane film.[103] The resulting MBs displayed high areal capacity of 0.72 mAh cm^{-2}, and outstanding flexibility without obvious capacity changes under different bending angles. Further, the as-assembled wearable integrated system based on monolithic Zn ion MBs and pressure sensor could achieve real-time health monitoring both statically and dynamically with high sensitivity. Although 2D in-plane Zn-ion MBs have made significant advances, a myriad of challenges still remain to be tackled before actual applications can be realized, including the further improvement of areal or volumetric energy/power density and cycling stability, suppression of the formation of dendritic zinc, enhancement of zinc plating/stripping columbic efficiency, optimization of electrolyte components for high stability, exploitation of flexible or self-healing electrolytes that are well comparable to ionic conductivity of liquid electrolyte, and development of scalable cost-effective technologies.

3.3. 3D In-Plane MBs

The key objective of the 3D in-plane MBs with interdigitated design is to enlarge areal loading of the footprint-confined active materials, notably boosting areal capacity and energy, in comparison with 2D in-plane microdevices. Moreover, 3D

hierarchical structure of microelectrode arrays is highly conducive for fast diffusion of electrolyte ions in the shortened 3D ion transfer pathways, which can simultaneously gain high areal power density and energy density. Typically, 3D interdigital nickel–zinc (Ni–Zn) MBs with high-aspect-ratio microelectrode arrays were fabricated by Chamran et al.[49] through photoassisted anodic etching and electroplating on the glass substrate. The photoassisted anodic etching was used to form deep hole in silicon mold template for the formation of the vertical microelectrodes, and the electroplating was implemented to fill the silicon mold with metal Ni and Zn. To prepare the microelectrodes of Ni–Zn MBs, $Ni(OH)_2$ as cathode was electrochemically deposited on the Ni microelectrode arrays. The as-obtained 3D interdigital Zn–$Ni(OH)_2$ MBs working in alkaline electrolyte exhibited relatively low areal capacity of 2.5 μAh cm^{-2} due to the low thickness of $Ni(OH)_2$ (1 μm). Afterward, Braun and co-workers[53] designed the mesostructured and isolated microelectrodes arrangement through 3D holographic lithography and conventional photolithography (**Figure 4**a–d). The uniform spatial distribution of microelectrode arrays and precise control of the internal electrode mesostructure endowed hierarchical and affluent channels for fast lithium-ion transport and increased the available active area limited by the given footprint. Therefore, the unique mesostructure enabled the fabricated full cells, based on Ni–Sn as anode and lithiated MnO_2 as cathode, to achieve ultrafast discharge rate up to 1000 C. As expected, high energy density of 6.5 μWh cm^{-2} $μm^{-1}$ and impressive power density of 3600 μW cm^{-2} $μm^{-1}$ were gained. This resulted from the advanced architecture of MBs through the elaborate design of the 3D conductive interdigital substrate and microelectrodes with rational size, shape, and porosity. Generally, the full optimization of the distribution, size, and ratio of length to diameter of vertically aligned microelectrodes is highly necessary for fast ion transfer, increasing active materials loading, and decreasing the device resistance, which can further improve energy density and power density. It is noteworthy that the fabrication of the most reported 3D MBs[49,50,104] basically relies on the well-established photolithography and electrodeposition techniques, rendering conventional electrode materials unusable. For instance, graphite, $Li_4Ti_5O_{12}$,

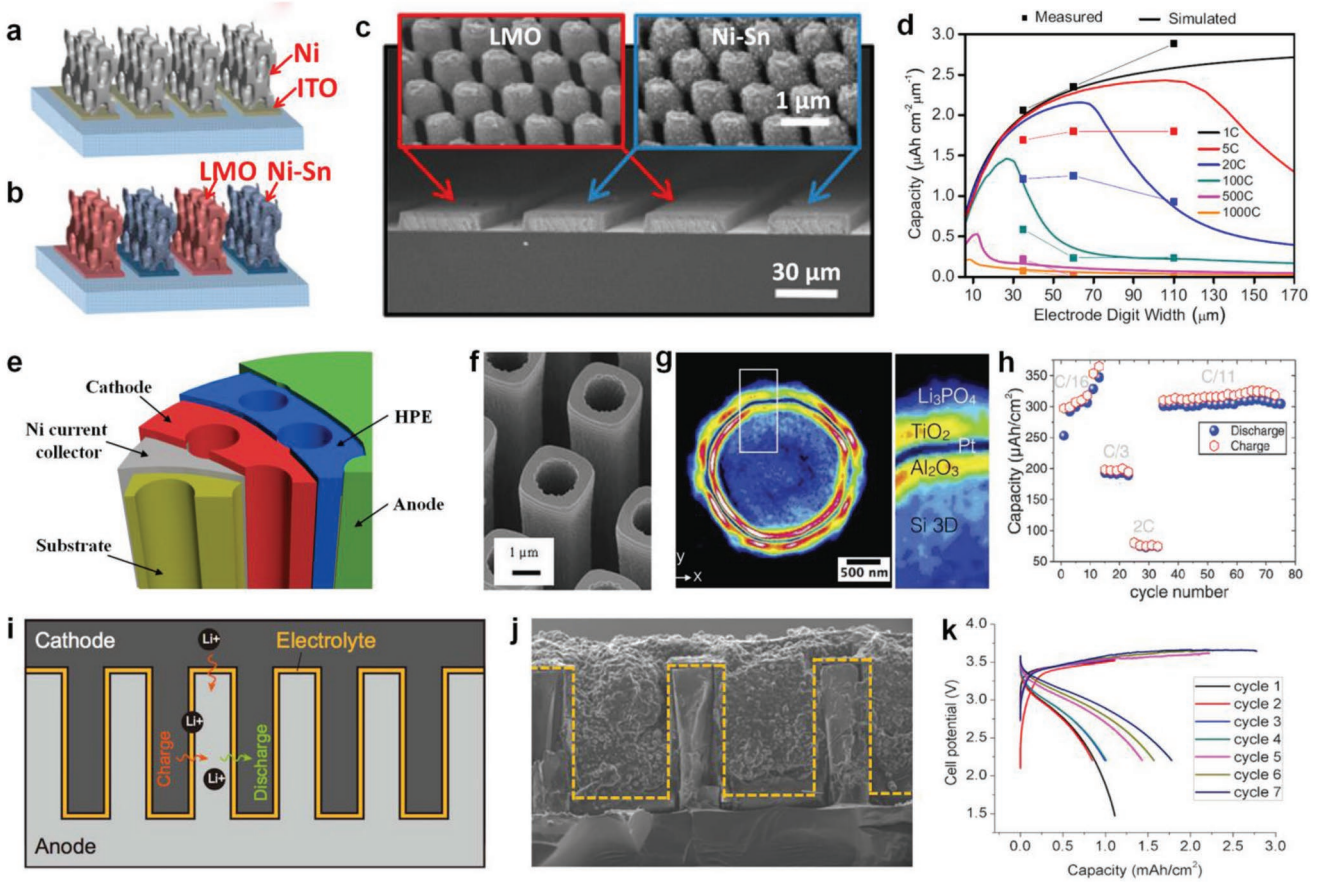

Figure 4. 3D in-plane and stacked MBs. a,b) Schematic of interdigital patterns of 3D in-plane MBs via electroplating of Ni–Sn and MnO_2, followed by lithiation to form lithiated MnO_2. c) Cross-section SEM image of the interdigital electrodes of 3D lithiated MnO_2 cathode (left inset) and Ni–Sn anode (right inset). d) Simulated (lines) and measured (scattered points) capacity as a function of electrode digit width. a–d) Reproduced with permission.[53] Copyright 2015, National Academy of Sciences. e) Schematic isometric view of the 3D stacked MBs based on conformal films of Ni current collector, MoS_2 cathode, hybrid polymer electrolyte, mesocarbon microbeads anode.[47] f) 3D silicon scaffold obtained from the selective reactive ion etching of the wafer. g) Top-view transmission X-ray microscopy image of the four functional layers deposited by ALD on silicon micropillars. h) Rate performance at different current densities. f–h) Reproduced with permission.[64] Copyright 2017, Wiley-VCH. i) Schematic diagram, j) cross-section SEM image, and k) charge–discharge profiles of 3D stacked lithium ion MBs. Reproduced with permission.[63] Copyright 2018, Elsevier.

$LiFePO_4$, $LiCoO_2$, $LiMn_2O_4$, and $LiNi_{05}Co_{0.3}Mn_{0.2}O_2$ are difficult to be directly synthesized on 3D interdigital current collectors. To solve this, a facile approach of colloidal suspension in a suitable solution followed by forced infiltration using silicon mold with deep holes was proposed for these conventional battery materials to construct 3D electrode arrays.[49] For example, mesocarbon microbeads (MCMBs) were used to assemble 3D carbon microelectrode arrays through the colloidal MCMBs dispersed in propylene carbonate to fill the perforated silicon mold. As a result, the 3D carbon microelectrodes lead to high areal capacity of 4.6 mAh cm^{-2}, about eight times greater than that of 2D microelectrodes (0.6 mAh cm^{-2}). The configuration of 3D microelectrodes enables the in-plane devices to accommodate more active materials with greatly enhanced areal capacity. Besides colloidal processing, the emerging 3D printing technique is highly flexible, which makes easy and elaborate design of on-chip 3D in-plane microelectrodes or current collector arrays on rigid or deformable substrates possible. This can be further used to deposit anode and cathode micropatterns of 3D MBs, holding great promise for flexible and wearable 3D in-plane microdevices.

3.4. 3D Stacked MBs

3D stacked MBs are capable of tapping the whole projected area of microelectrodes by utilizing the third dimension (with height up to 500 μm), allowing for high active material loading and enhanced areal capacity, in comparison with 2D stacked MBs in the fixed footprint area. Therefore, such 3D MBs could deliver intrinsically high areal energy density via rational fabrication. For instance, Nathan et al.[47] reported full 3D stacked MBs on a perforated substrate (silicon and glass), with the conformal films of electroless-deposited Ni current collectors (2–4 μm), electrodeposited MoS_2 cathode (1 μm), hybrid PVDF polymer/SiO_2 electrolyte membrane, mesocarbon microbeads as both anode and current collector to fill the remaining cylindrical cavities by spin-coating and vacuum pulling method (Figure 4e). The areal capacity of this cell reached up to 2 mAh cm^{-2}, 30 times higher than that of 2D stacked MBs with the same device components, because of substantial microchannel plates on substrate providing tremendously increased surface area for mass loading. After that, Lethien and co-workers[64] developed 3D stacked MBs based on four functional layers, consisting of insulating thin film (Al_2O_3), current collector (Pt), negative electrode (TiO_2), and solid electrolyte (Li_3PO_4), on 3D scaffolds of double microtubes at the silicon wafer through ALD (Figure 4f–h). Due to the significantly enlarged geometrical surface, an increased areal capacity from 3.5 up to 370 μAh cm^{-2} was obtained. Most previous works reported used silicon substrates as only scaffold to load up active materials, resulting in relatively low fraction of active materials and small capacity. Recently, a new fabrication route for all-solid-state 3D stacked MBs was developed by Dunn and co-workers[63] based on semiconductor processing method and photopatternable polymer electrolyte derived from SU-8 photoresist to form conformal solid-state electrolyte (Figure 4i–k). 3D silicon anode made by dry etching crystalline silicon wafers was served as both the scaffold and negative electrode. The resultant silicon anode was subjected to partial lithiation (10% of theoretical capacity) to keep volume change controlled during charge and discharge. Conformal electrolyte with micrometer-thick layer derived from SU-8 photoresist gave lithium ionic conductivity of 2.8×10^{-7} S cm^{-1}. It was found that longer exposure time for cross-linked SU-8 decreased ionic conductivity. Vacuum-infiltrated approach was used to form the stacked cathode of $LiNi_{0.8}Co_{0.15}Al_{0.05}O_2$. The rechargeable 3D stacked MBs in a small-format 3 mm × 3 mm footprint delivered high areal capacity of 1.8 mAh cm^{-2} and remarkable areal energy density of 5.2 mWh cm^{-2}. Furthermore, such microdevices could be operated at a high current density of 0.66 mA cm^{-2} with good cycling performance. Even though these 3D microelectrodes can deliver high areal capacity, few designs of the full 3D stacked MBs have been realized so far, resulting from the intractable technical factor of uniform conformal layer-by-layer deposition on 3D topologies. The utilization of substrate (silicon and carbon) as both active materials and supports would be a highly reliable way to simplify the fabrication processing and decrease the fraction of inactive materials. Taking account of huge demands for consumer microelectronics and appearance of internet of things, 3D stacked MBs with high areal capacity will become the popular microscale power supplies for various microsystems in the future.

4. Micro-Supercapacitors

MSCs, as novel microscale energy storage devices, have attracted much attention due to high power density (≈10^3 W cm^{-3}), robust rate capability (up to 10^3–10^4 V s^{-1}), and ultralong cyclability (≈10^6 cycles).[2,105–109] **Figure 5** shows the development history and advances of MSCs from 2D to 3D microelectrode structure with the introduction of new microfabrication technologies, as well as being accompanied by the continuous improvement of flexibility and stretchability. **Table 2** gives a summarization of the areal and volumetric electrochemical performances of the various planar MSCs based on different electrode materials.

4.1. 2D Stacked MSCs

The architecture and merits of 2D stacked MSCs are very similar to the aforementioned stacked MBs. The primary obstruction for such thin-film MSCs substantially originates from low ionic conductivity of solid electrolyte, which dramatically limits power and energy densities, and eventually inhibits the applications in microsystems. So far, only a few works of such stacked MSCs have been reported using LiPON (10^{-6} S cm^{-1}) as solid electrolyte/separator and RuO_2 as electrodes through multistep sputtering strategy.[118,129,130] Recently, several 2D materials with relatively high ionic conductivity have been discovered, such as GO,[131] boron nitride (BN),[132] and vermiculite.[133] The ionic conductivity of these 2D materials can reach up to 10^{-3}–10^{-2} S cm^{-1} in low concentration salt solution due to much abundant hydrophilic functional groups on their surface. Moreover, the intrinsic 2D structure enables them to readily form ultrathin film with a thickness of ≤100 nm. These two merits endow such 2D materials as a promising separator for assembling 2D

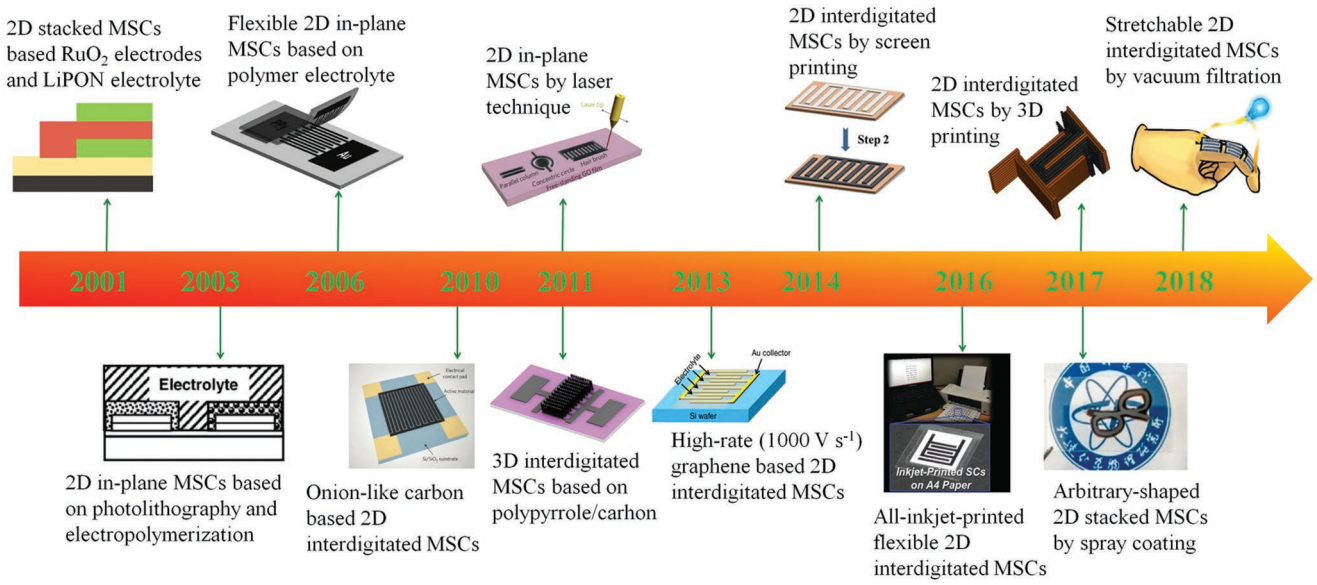

Figure 5. A brief timeline showing the history of development of various planar MSCs. Inset images: "2D in-plane MSCs based on photolithography and electropolymerization." Reproduced with permission.[110] Copyright 2003, Elsevier. "Flexible 2D in-plane MSCs based on polymer electrolyte." Reproduced with permission.[111] Copyright 2006, Elsevier. "Onion-like carbon based 2D interdigitated MSCs." Reproduced with permission.[112] Copyright 2010, Nature Publishing Group. "3D interdigitated MSCs based on polypyrrole/carbon." Reproduced with permission.[113] Copyright 2011, Elsevier. "2D in-plane MSCs by laser technique." Reproduced with permission.[45] Copyright 2011, Nature Publishing Group. "High-rate (1000 V s^{-1}) graphene based 2D interdigitated MSCs." Reproduced with permission.[114] Copyright 2013, Nature Publishing Group. "2D interdigitated MSCs by screen printing." Reproduced with permission.[115] Copyright 2014, Royal Society of Chemistry. "All-inkjet-printed flexible 2D interdigitated MSCs." Reproduced with permission.[29] Copyright 2016, Royal Society of Chemistry. "2D interdigitated MSCs by 3D printing." Reproduced with permission.[116] Copyright 2017, American Chemical Society. "Arbitrary-shaped 2D stacked MSCs by spray coating." Reproduced with permission.[46] Copyright 2017, American Chemical Society. "Stretchable 2D interdigitated MSCs by vacuum filtration." Reproduced with permission.[117] Copyright 2018, Elsevier.

stacked MSCs. As a typical example, our group applied nano-sized GO (NGO, lateral size of 100 nm) as a separator for the construction of all graphene-based arbitrary-shape stacked MSCs, such as junction-wire shape, hollow square shape, letter shapes, and number shapes, on a flexible substrate through layer-by-layer spray coating approach (**Figure 6**a).[46] The flexible NGO separator with a thickness of ≈2 µm exhibited an improved capacitance thanks to much more ordered water near the confined NGO layers, and exceptional ionic conductivity that is well comparable to the gel electrolyte of polyvinyl alcohol (PVA)/H_2SO_4. Because of the compatible interface and strong interaction between GO and graphene, the as-fabricated MSCs presented excellent flexibility and electrochemical stability even under serious bending and twisting deformation (Figure 6b,c). It should be noted that this is the first realization of arbitrary-shaped flexible stacked MSCs. Further, 2D BN nanosheets were used as a new-type separator (≈2.2 µm), sandwiched between MnO_2 nanosheet/PH1000 cathode layer and graphene anode layer, to manufacture asymmetric stacked MSCs on various flexible substrates, using the same spray coating technology.[119] The resulting asymmetric MSCs exhibited stable electrochemical stability at high voltage of 1.8 V and impressive energy density of 8.6 mWh cm^{-3}. Despite the crucial advance of the stacked MSCs using GO and BN nanosheets as separators, it is still unclear what the transport mechanism of electrolyte ions on the surface of these 2D materials is, how the thickness of both electrodes and ultrathin separator affects the electrolyte ions diffusion, and whether the different functional groups on the surface of these 2D nanosheets influence the ionic conductivity. Nevertheless, designing hybrid thin film microelectrodes with 2D nanosheets and heterostructures could provide numerous ways for creating high-capacitance microdevices in a confined area or volume.[134,135] It is believed that, with assistance of high-resolution printing techniques, graphene and 2D materials, serving as both active materials and innovative ultrathin-separators (<1 µm), will open various opportunities to develop ultrathin, flexible, and integrated MSCs with stacked geometry.

4.2. 2D In-Plane MSCs

2D in-plane MSCs, with extremely short ionic pathway ranging from several to hundreds of micrometers, are one class of highly competitive complementary miniaturized yet robust energy supply. From 2003, Sung et al.[110,111,136] have developed the prototypes of 2D in-plane MSCs to all-solid-state MSCs and flexible MSCs based on electrochemical polymerized polypyrrole (PPy) electrodes, using H_3PO_4/PVA and organic $LiCF_3SO_3$/polyacrylonitrile gel electrolyte. After that, various innovative strategies have been well developed for the fabrication of such MSCs with high-precision microelectrodes, such as photolithography,[137,138] plasma-etching process,[114] laser technique,[44,139] electrochemical deposition,[112,140] and printing techniques.[29,34,141] Furthermore, a great lot of nanostructured electrochemically active materials were ingeniously designed for high-performance MSCs, for example, onion-like carbon,[112]

Table 2. Summary of the electrochemical performance of various planar MSCs. C_A: Areal capacitance. C_V: Volumetric capacitance. HQ: Hydroquinol. OLC: Onion-like carbon. PC: Propylene carbonate. EMIMTFSI: 1-ethyl-3-methylimidazolium bis(trifluoromethylsulfonyl) imide. G: Graphene. FG: Fluorine-modified graphene. AG: Activated graphene. $EMIMBF_4$: 1-ethyl-3-methylimidazolium tetrafluoroborate. LDH: Layer double hydroxides. PANI: Polyaniline. CMC: Sodium carboxymethylcellulose.

Types	Electrodes	Thickness [μm]	Electrolyte	V	C_A [mF cm^{-2}]	C_V [F cm^{-3}]	E_A [μWh cm^{-2}]	P_A [mW cm^{-2}]	E_V [mWh cm^{-3}]	P_V [W cm^{-3}]	Stability	Refs.
2D stacked MSCs	RuO_2//RuO_2	0.3//0.3	LiPON	0–2	38[a]	–	21[c]	–	–	–	500 (53%)	[118]
	EG//EG	0.7//0.7	H_2SO_4/PVA	0–0.8	3.3[a]	10.6[a]	0.29[c]	0.76[c]	0.98[a]	2.1[a]	10 000 (93%)	[46]
	EG-HQ// EG-HQ	0.7//0.7	H_2SO_4/PVA	0–0.8	9.8[a]	32.7[a]	0.87[c]	–	2.9[a]	2.3[a]	–	[46]
	EG// MnO_2-PH1000	1.8//0.9	LiCl/PVA	0–1.8	9.6[a]	19.2[a]	4.3[c]	–	8.6[a]	4.2[a]	5000 (92%)	[119]
2D in-plane MSCs	OLC//OLC	7//7	Et_4NBF_4/PC	0–3	–	1.3[b]	–	–	1.6[b]	200[b]	10 000 (100%)	[112]
	LSG//LSG	7.6//7.6	H_2SO_4/PVA	0–1	2.3[a]	3[a]	0.3[c]	–	0.4[a]	60[a]	10 000 (96%)	[44]
	LSG//LSG	7.6//7.6	EMIMTFSI	0–2.5	–	2.3[a]	–	–	2.1[a]	140[a]	30 000 (100%)	[44]
	Ti_3C_2//Ti_3C_2	1.3//1.3	H_2SO_4/PVA	0–0.6	27[b]	357[b]	1.3[c]	–	18[b]	15[b]	10 000 (110%)	[120]
	CDC//CDC	1.4//1.4	1 M H_2SO_4	0–0.9	12[c]	87[c]	1.5[b]	30[b]	11[b]	250[b]	–	[3]
	rGO//rGO	0.015//0.015	H_2SO_4/PVA	0–1	80[b]	18[b]	11.1[c]	–	2.5[b]	495[b]	100 000 (100%)	[114]
	PANI-G/EG// PANI-G/EG	4.5//4.5	$EMIMBF_4$	0–2.5	34[b]	69[b]	29[c]	–	46[b]	6.4[b]	–	[121]
	FG//FG	0.7//0.7	$EMIMBF_4$/ PVDF-HFP	0–3.5	4.4[b]	33.5[b]	7.4[c]	–	56[b]	21[b]	5000 (93%)	[122]
	LSG–MnO_2// LSG–MnO_2	15//15	1 M Na_2SO_4	0–0.9	400[a]	250[a]	45[c]	–	30[a]	10[a]	–	[123]
	$Li_4Ti_5O_{12}$//AG	3//10	LiTFSI/P_{14}TFSI/ PVDF-HFP	0–3	27.8[b]	42.8[b]	35[c]	–	53.5[b]	3.5[b]	6000 (99%)	[27]
	Ti_3C_2// Co–Al–LDH	–	6 M KOH	0.4–1.45	40[b]	–	10.8[b]	8.8[b]	–	–	10 000 (92%)	[124]
	Zn//AC	50//80	$ZnSO_4$/CMC	0.5–1.5	1297[b]	–	115.4[b]	4[b]			10 000 (100%)	[125]
	MnO_2–PPy// V_2O_5–PANI	–	LiCl/PVA	0–1.6	–	55.7[b]	–	–	19.8[b]	2.6[b]	7000 (92%)	[126]
3D in-plane MSCs	G-CNTs//G-CNTs	15//15	1 M Na_2SO_4	0–1	2.1[b]	1[b]	0.3[c]	–	0.15[b]	115[b]	–	[127]
	G-CNTs//G-CNTs	20//20	$BMIMBF_4$	0–3	3.9[b]	2[b]	4.9[c]	–	2.4[b]	135[b]	8000 (98%)	[127]
	MnO_2//MnO_2	68//68	0.5 M Na_2SO_4	0–0.8	113[a]	–	10[a]	20[a]	–	–	–	[128]

[a]Reported values based on footprint area or volume of device; [b]Reported values based on electrode area or volume. The thickness referred to the whole anode and cathode; [c]Calculated values according to the reported literatures.

carbide-derived carbon,[26] graphene (reduced GO, doped graphene, and laser-scribed graphene (LSG)),[28,105,123,139,142] GO,[143] MXene,[144–146] MoS_2,[147,148] and their hybrids with pseudocapacitive metal oxide (e.g., MnO_2 and RuO_2)[149,150] and conducting polymers (polyaniline).[121,151,152] Among them, 2D materials, e.g., graphene and MXene, with large exposed surface area and abundant accessible active sites are well matched to the in-plane architecture of MSCs, in which electrolyte ions can transfer in parallel along the flat plane of 2D materials with minimization of the diffusion barriers, and make full use of atomic layer thickness of 2D materials to adequately boost electrochemical performance (Figure 6d).[114,153–155] Moreover, 2D materials intrinsically possess mechanical robustness to endow them as microelectrodes for the interdigital flexible MSCs with outstanding stretchability and self-repairability when self-recovering gel electrolyte is used.

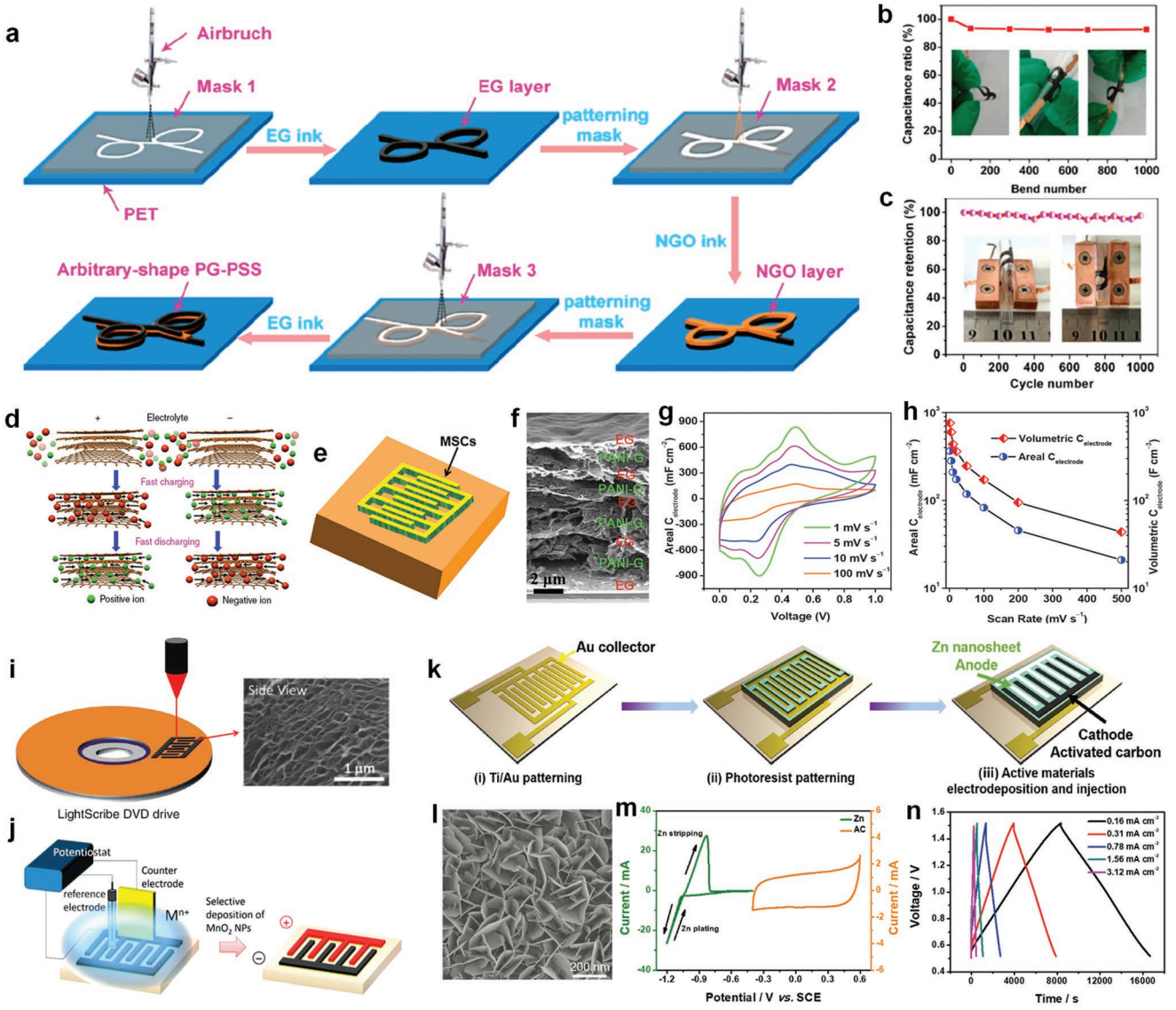

Figure 6. 2D stacked and in-plane MSCs. a) Schematic of the fabrication of 2D stacked junction-wire-shaped MSCs. b) Capacitance retention as a function of repeated bending number. Insets are three bending states. c) Cycling stability under a severe bending condition. Insets are top- and side-view optical images of junction-wire-shaped MSCs. a–c) Reproduced with permission.[46] Copyright 2017, American Chemical Society. d) In-plane geometry of graphene-based MSCs, showing that the ions between the electrode gaps can be rapidly transported along the planar graphene sheets with a short diffusion pathway. Reproduced with permission.[114] Copyright 2013, Nature Publishing Group. e) Schematic diagram, f) cross-section SEM image of microelectrode, g) CV curves, h) areal and volumetric capacitance of 2D interdigital MSCs based on nanohybrid stacked film. e–h) Reproduced with permission.[121] Copyright 2015, Wiley-VCH. i) Schematic of the fabrication of 2D interdigital MSCs from LSG. Reproduced with permission.[44] Copyright 2013, Nature Publishing Group. j) Schematic of asymmetric MSCs based on LSG negative electrode and LSG–MnO_2 positive electrode via electrochemical deposition. Reproduced with permission.[123] Copyright 2015, National Academy of Sciences. k) Schematic of the fabrication process of planar ZIMCs. l) SEM image of electrodeposited Zn nanosheets as anode. m) CV curves of Zn anode and AC cathode. n) Charge–discharge curves obtained at different current densities. k–n) Reproduced with permission.[125] Copyright 2018, Wiley-VCH.

Ti_3C_2 MXene presents high volumetric capacitance of up to ≈1500 F cm^{-3}, surface hydrophilicity, and metallic conductivity of ≈9000 S cm^{-1},[156–159] which has been acknowledged as an attractive candidate for 2D in-plane MSCs. Typically, Gogotsi and co-workers[120] fabricated all-MXene solid-state 2D in-plane MSCs using large-flake MXene (lateral size of 3–6 μm) as current collectors and small-flake MXene (≈1 μm) as active material through spray coating technique, followed by direct laser cutting approach. Benefited by the high conductivity of large-flake MXene and abundant active sites of small-flake MXene, the resulting all-MXene MSCs exhibited high volumetric capacitance of 356.8 F cm^{-3}, but the cell voltage in aqueous electrolyte is very limited, only 0.6 V, showing a low energy density of 18 mWh cm^{-3}. To address this issue, our group developed high-voltage ionogel-based MSCs based on the same ionic liquid preintercalated MXene films in 1-butyl-3-methylimidazolium tetrafluoroborate ($EMIMBF_4$). The as-fabricated MXene-based MSCs stably worked at a voltage of 3 V

in $EMIMBF_4$/PVDF-HFP electrolyte, and delivered remarkable energy density of 43.7 mWh cm^{-3}.[160] Therefore, it is concluded that, through further optimization of MXene flake size, thickness, composition, and selective screening of high-voltage and stable electrolyte, the capacitive performance of MXene-based MSCs can be tremendously enhanced.

Graphene has been considered as an ideal electric double layer capacitive material because of ultrathin flexible structure, high surface area (2630 m^2 g^{-1}), superior electrical conductivity, and high theoretical capacitance (550 F g^{-1}).[161–163] However, the electrochemical performance has been primarily hindered by the restacking tendency due to strong Van der Waal force between graphene nanosheets, resulting in the huge decrease of accessible surface area of electrolyte ions. To address this issue, one reliable strategy is to efficiently hybridize nanospacers to minimize Van der Waal force of graphene nanosheets and improve the ionic accessibility. For instance, Wu et al.[121] constructed a micrometer-thick compact hybrid film based on alternating stacked mesoporous polyaniline-functionalized graphene and EG, with layered sandwich structure, for MSCs (Figure 6e–h). Taking into account the positive synergistic effect, polyaniline based graphene nanosheets can not only prevent the restacking of graphene but also provide tremendous pseudocapacitive contribution to greatly improve the capacitance. Consequently, the assembled MSCs delivered landmark volumetric capacitance of 736 F cm^{-3} in aqueous electrolyte and ultrahigh energy density of 46 mWh cm^{-3} in ionic liquid. On the other hand, another approach is to design and create hierarchical pores between graphene nanosheets to directly avert the restacking, increase the accessible area, and reduce the barriers of ion diffusion. For example, Kaner and co-workers[44,164] employed an infrared laser to reduce the stacked GO film into well-exfoliated graphene (LSG) film by an unusual photothermal effect, in which GO strongly absorbs high-intensity light to primarily remove functional groups on its surface (Figure 6i). The as-fabricated LSG electrodes had notable features like excellent electrical conductivity of 2.35×10^3 S m^{-1}, open network structure, and high surface area of 1520 m^2 g^{-1}. As a result, the interdigital MSCs delivered a significant increase of energy density and power density, compared with active carbon-based supercapacitors. Furthermore, the resultant LSG microelectrodes could be used as conducting substrates for the deposition of high-capacitance pseudocapacitive materials, and subsequent assembly of symmetric MSCs or asymmetric MSCs (Figure 6j).[123] For instance, MnO_2 was deposited onto the surface of LSG microelectrodes with open porous structure and high surface area. As a consequence, the hybrid LSG–MnO_2 electrodes possessed ultrahigh volumetric capacitance of over 1100 F cm^{-3}. When it was converted to the constituent MnO_2, this capacitance value corresponded to 1145 F g^{-1}, approaching the theoretical value of 1380 F g^{-1}. Therefore, the exploitation of novel 2D hybrid nanosheets with enriched exposed edges, tailored thickness, and well-defined nanopores can dramatically improve areal/volumetric capacitance and rate capability of planar MSCs.

Besides the consideration of intrinsic capacitance of electrode materials, another key factor regarding high energy density of MSCs is the applied voltage because the energy density is proportional to the square of the cell voltage. In this case, developing high-voltage electrolytes, e.g., water-in-salt electrolyte,[91,165] ionic liquid,[166] and organic electrolyte,[3] and the reasonable construction of aqueous asymmetric devices[167,168] and hybrid energy storage devices to enlarge cell voltage window are the key approaches for improving energy density of MSCs. As a typical example, our group recently reported ionogel-based fluorine-modified graphene (FG) MSCs with the $EMIMBF_4$/PVDF-HFP electrolyte.[122] Since the FG films exhibited enriched fluorine modified electrochemically active sites, high electrical conductivity, and compatible interfacial wettability between microelectrodes and $EMIMBF_4$/PVDF-HFP electrolyte with a wide voltage of 3.5 V, the as-fabricated MSCs showed impressive volumetric capacitance of 134 F cm^{-3} and ultrahigh energy density of 56 mWh cm^{-3}.

To boost the energy density, developing asymmetric planar MSCs with suitably matched pseudocapacitive electrode and electrical double-layer capacitive electrode is also a good choice to improve the capacitance and cell voltage. For instance, Yang and co-workers[169] developed the asymmetric MSCs based on interdigitated microelectrodes of vanadium pentoxide and graphene-vanadium nitride quantum dots via 3D printing strategy to simultaneously realize the efficient patterning and high loading of active materials. Remarkably, the as-printed asymmetric MSCs with a cell voltage of 1.6 V presented high areal capacitance of 208 mF cm^{-2} and energy density of 74 μWh cm^{-2}. However, the printed thick microelectrodes suffer from low electronic conductivity, poor rate capability, and inferior cycling stability. Zhang and co-workers[170] prepared a series of sandwich-structured transition metal hexacyanoferrates (MHCF, M = Cu, Ni, Co, and Fe)/graphene thin films for asymmetric MSCs by alternate stacking deposition of graphene and MHCF layers. Thanks to the structural advances of hybrid films and asymmetric in-plane configuration, the resultant MSCs based on FeHCF as anode and CuHCF as cathode offered high energy density of 44.6 mWh cm^{-3}.

Hybrid ion microcapacitors, e.g., lithium ion microcapacitors (LIMCs) and zinc ion microcapacitors (ZIMCs), can sufficiently combine the merits of capacitive electrode and battery-type electrode, simultaneously delivering high energy density and high power density. Recently, our group developed all-solid-state planar LIMCs with interdigital patterns of lithium titanate (LTO) nanospheres as anode and activated graphene (AG) as cathode through mask-assisted filtration of electrode materials and EG.[27] By coupling with high-voltage ionogel electrolyte, the as-assembled LIMCs delivered high volumetric energy density of 53.5 mWh cm^{-3}, stable cycling performance with 98.9% of capacitance retention after 6000 cycles, high safety at high temperature of 80 °C, outstanding flexibility, and modular integration of bipolar cells. The exceptional performance of these LIMCs was mainly attributed to the synergistic combination of the advances of the stacked-layer microelectrodes with in-plane geometry, effective match of zero-strain Faradaic LTO and high-capacitance non-Faradaic AG, strong interfacial engineering between the microelectrodes and substrate with the help of large-lateral-size EG nanosheets as 2D conducting additive, and flexible support. As another example, Feng and co-workers[125] constructed the planar ZIMCs, made of electrodeposited Zn nanosheets as anode and activated carbon (AC) as cathode via the incorporation of photolithography, electrodeposition,

and injection (Figure 6k–n). Thanks to the reversible stripping/plating of the Zn anode and fast ion adsorption/desorption on the AC cathode, the resulting ZIMCs achieved record areal capacitance of 1200 mF cm^{-2}, areal energy density of 115.4 μWh cm^{-2}, and excellent cycling stability without obvious decay after 10 000 cycles. Meanwhile, Qu and co-workers[171] reported the flexible planar ZIMCs based on Zn anode and CNTs cathode through electrodeposition. The as-obtained ZIMCs delivered high areal energy and power densities of 29.6 μWh cm^{-2} and 8 mW cm^{-2}, respectively, and achieved remarkable flexibility without capacitance decay bent from flat to 180°. Moreover, the degraded ZIMCs could be restored by replenishing the zinc source without destroying original configuration to enhance the capacitance and longevity. Therefore, designing asymmetric MSCs and hybrid ion microcapacitors is an effective strategy to improve the energy density of MSCs. However, the R&D of asymmetric MSCs and hybrid ion microcapacitors has not been completely exploited, due to the huge challenges of the mass/charge balance of anode and cathode, kinetic match of Faradaic and non-Faradaic reaction, screen of suitable electrolyte, and interfacial integrity of microelectrodes with electrolyte and current collectors.

One of the greatest performance metrics of 2D in-plane MSCs is that they usually present ultrahigh frequency response with alternating current (AC) line-filtering,[96] accounting for filtering AC into direct current (DC). In principle, AC line-filtering requires a resistor–capacitor (RC) constant of less than 8.3 ms (120 Hz).[172,173] The state-of-the-art interdigital MSCs could deliver a RC constant of less than 1 ms, superfast scan rate up to 1000 V s^{-1} or more (10 000 V s^{-1}),[107,137,152] indicative of ultrahigh instantaneous power delivery. Typically, as reported by Wu et al.,[105] it involved the bottom-up fabrication of continuous and ultrathin sulfur-doped graphene (SG) films derived from the peripheral trisulfur-annulated hexa-peri-hexabenzocoronene (SHBC) through thermal annealing with assistance of a thin Au protecting layer (**Figure 7**a). After the deposition of gold current collectors and oxidative etching, 2D in-plane MSCs based on SG films were achieved. Due to the uniform S doping, high conductivity of SG film, and short ionic transfer distance, the fabricated planar MSCs could work at ultrafast scan rate of 2000 V s^{-1} (Figure 7b), simultaneously delivering a remarkable capacitance of 8 F cm^{-3} at that scan rate. The discharge current density of the MSCs linearly responds to the scan rate of up to 2000 V s^{-1}. The microdevices exhibited a large characteristic frequency of 3836 Hz at the phase angle of −45°, corresponding to a short time constant of 0.26 ms, indicative of ultrafast frequency response. Furthermore, these devices offered an ultrahigh power density of 1191 W cm^{-3}, which was well comparable to that of Al electrolytic capacitors. Zhu and co-workers[107] reported the fabrication of flexible multilayered graphene-based MSCs

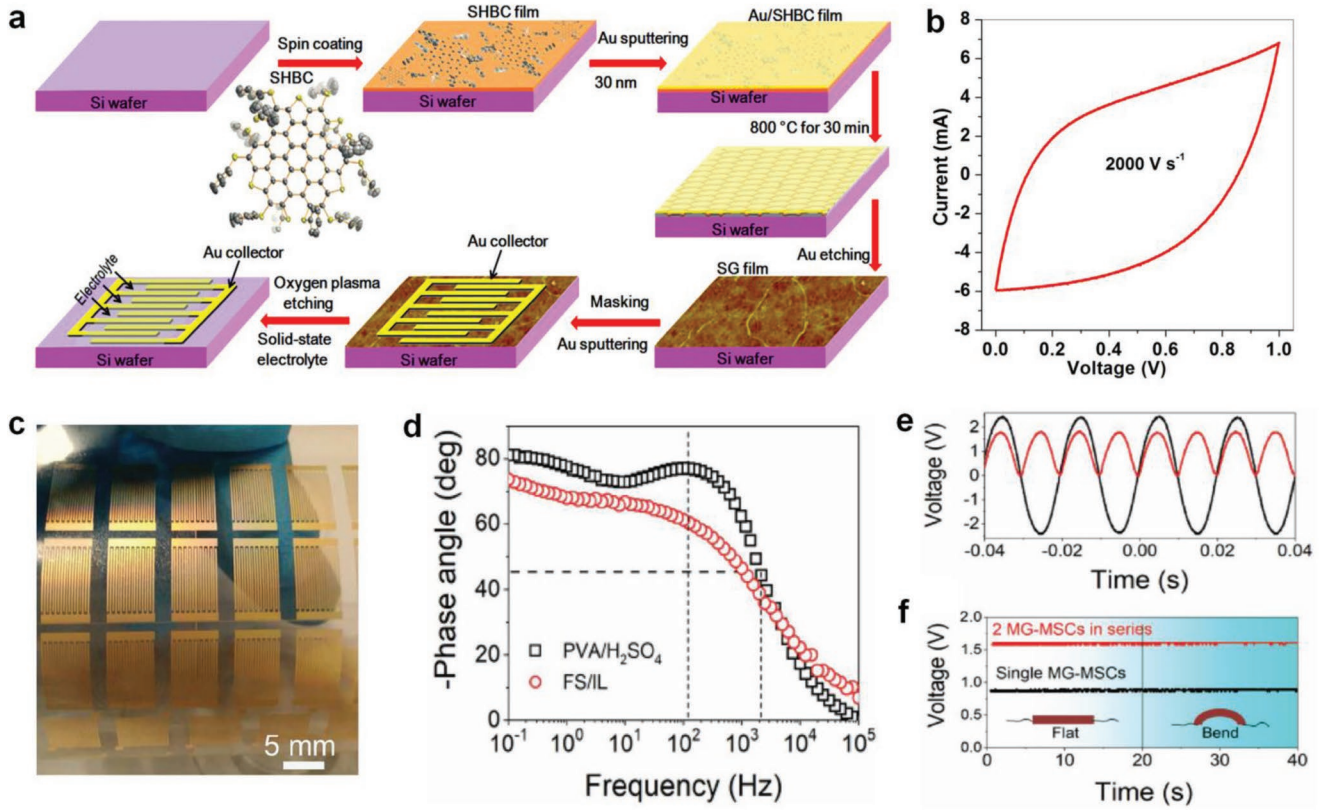

Figure 7. 2D in-plane MSCs with AC line filtering performance. a) Schematic diagram of SHBC-derived SG films for MSCs on a Si/SiO_2 wafer. b) CV curves at scan rate of 2000 V s^{-1}. a,b) Reproduced with permission.[105] Copyright 2017, American Chemical Society. c) Photograph of CVD graphene MSCs arrays on flexible substrate. d) Phase angle as a function of the frequency. e) AC input signal and pulsating DC signal converted by bridge rectifier. f) DC signal output of CVD graphene MSCs in series under flat and bending states. c–f) Reproduced with permission.[107] Copyright 2018, Wiley-VCH.

with AC line-filtering performance, using dry transfer and direct laser writing of highly electrical conductive CVD graphene (Figure 7c). Benefitting from the increased interlayer distance, efficient ion/electron conducting channels, high conductive microelectrodes, and narrow interspace, the characteristic frequency at phase angle of −45° was 2025 Hz with a short time constant of 0.49 ms (Figure 7d). At 120 Hz, the phase angle was −76.2°, corresponding to an ultralow RC time constant of 0.54 ms. Furthermore, an AC line-filtering electrical circuit was designed, where a full wave bridge rectifier, the fabricated MSCs, and a load resistor were contained. It was demonstrated that pulsating DC signal generated by bridge rectifier (Figure 7e) was readily converted into the stable and smooth DC output of 0.88 V for one cell and 1.6 V for two cells of MSCs (Figure 7f). Even though the circuit was subjected to severe deformation, the DC output was stably unchanged, indicative of great potential of such MSCs for AC line-filtering applications. Benefitting from higher energy and prominent miniaturization compared to Al electrolytic capacitors, the largest component in most integrated circuits, such 2D in-plane MSCs, can potentially replace the bulky electrolytic capacitors to apply for miniaturized and integrated electronics.

4.3. 3D In-Plane MSCs

To further improve areal capacitance and energy density, developing 3D in-plane MSCs with increased areal loading of active materials is regarded as an effective way. Moreover, 3D microelectrode arrays can not only accelerate electrolyte ions diffusion into/out from the abundant nanochannels of microelectrodes but also significantly increase accessible active sites of active materials to the electrolyte, contributing to enhanced areal energy and power densities. To this end, Lin et al.[127] designed 3D CNT carpets based MSCs on interdigital graphene micropatterns through multistep CVD process, in which in situ growth of CNTs on graphene enabled them to seamlessly join each other, and thereby form well-developed electrically conducting network and affluent channels for electrolyte ions diffusion (**Figure 8**a–d). As a result, the as-fabricated MSCs showed ultrahigh rate capability up to 500 V s^{-1} (Figure 8e), AC line-filtering performance (Figure 8f), exceptional power density of 115 W cm^{-3}, and two orders of magnitude higher energy density than Al electrolytic capacitors. As another typical example, 3D microelectrode arrays were applied as a support to load MnO_2 film with a homogeneous thickness of 350 nm (Figure 8g).[128] With these 3D microelectrode scaffolds,

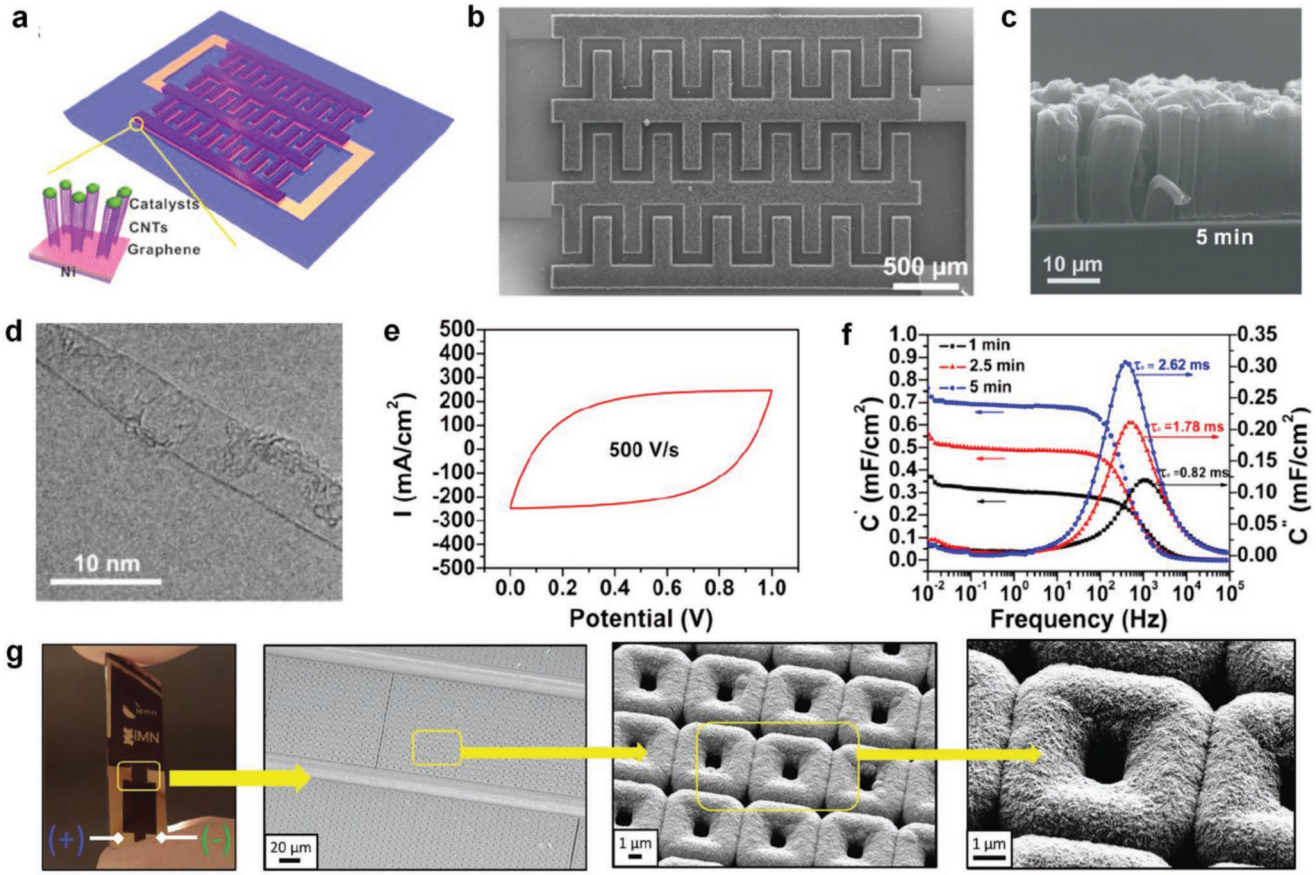

Figure 8. 3D in-plane MSCs. a) Schematic of graphene/CNT carpets (G/CNTCs) MSCs grown by CVD technique. b) Top-view SEM image of G/CNTCs-MSCs. c) Cross-section SEM image of G/CNTCs-MSCs. d) Transmission electron microscopy image of single CNT. e) CV curve at scan rate of 500 V s^{-1}. f) Evolution of the real and imaginary capacitance as a function of frequency. a–f) Reproduced with permission.[127] Copyright 2013, American Chemical Society. g) Overview of 3D MnO_2 interdigital MSCs from macroscopic view down to nanometer scale. Reproduced with permission.[128] Copyright 2017, Wiley-VCH.

the assembled MSCs delivered high areal energy density of ≈10 μWh cm^{-2} and power density of ≈1 mW cm^{-2} simultaneously, suggestive of great promise for on-chip electronics. However, these used technological processes, e.g., CVD and photolithography, for constructing 3D interdigitated topology involve complicated multiple steps with high cost. To overcome this, the emerging 3D printing[174] and laser technologies[175] could offer the possibility of fast and scalable fabrication of 3D interdigitated microelectrode arrays, with easy operation and high resolution, from 3D active electrodes to high-conductive 3D current collectors for MSCs. In general, the manufacturing of symmetric 3D interdigital MSCs with two identical microelectrodes is much simpler than those of asymmetric MSCs or MBs with two different electrode material fingers. Although 3D geometry is an intriguing approach to effectively increase areal capacitance and energy density of MSCs, the parameters (size, length, and width) and hierarchical structure (surface, pores, and functionalities) of 3D microelectrodes still lack the systematic investigation to maximize the electrochemical performance. Furthermore, such in-plane 3D MSCs in principle do not fully use their architecture merits to pack high-loading active materials for achieving high areal capacitance while maintaining fast ion transfer and power density. To further improve energy density, the creation of 3D interdigital hybrid MSCs with asymmetric microelectrodes is a feasible strategy thanks to the enlarged cell voltage (e.g., 2–4 V) and introduction of pseudocapacitive materials for enlarging areal or volumetric capacitance. Unfortunately, there is still no 3D stacked MSCs reported so far, inhibited by the technical complexity of cell configuration and low ionic conductivity of conformable solid-state electrolyte. Similar to 3D stacked MBs, exploiting printable, bendable, shape-conformable polymer gel electrolytes with high ionic conductivity would be a good option to build novel 3D stacked MSCs.

5. Integration for Flexible Standalone System

The continuous growth of miniaturized flexible electronics has intensively stimulated the ever-increasing pursuits of highly integrated standalone systems with long durability and free maintenance.[7,176–178] Miniature energy harvesters as power supplies, e.g., photovoltaic cell[179] or nanogenerator,[17] usually cannot generate sufficient electricity to power the microelectronic devices for long-time operation, due to their discontinuity, indeterminacy, and low efficiency. The combination of miniaturized energy harvester and microscale energy storage devices into a self-powered system is regarded as an efficient route to remedy the insufficient power generated by energy harvesters and solve the issue of electricity source for MEESDs. For instance, carbon based MSCs were integrated with a solar panel and an in-plane integrated circuit on a flexible polymer substrate to realize self-powering.[180] Integrating triboelectric nanogenerator with MXene-based MSCs for wearable harvester-storage module was used as highly compact self-charging power unit.[15] Zn//$LiFePO_4$ MBs to combine thermo-electrochemical cell scavenging body heat energy realized a wearable self-charging system.[55] As far as the functionalized smart standalone systems are concerned, one very promising direction is to integrate the different microdevices of energy generation, energy storage, and energy consumption on a single flexible substrate into a complete standalone system, such as, self-powered implantable biomedical device, environmental sensor, and health monitor. These self-sufficient microsystems with self-powered and intelligent functions can convert energy harvested from surrounding environment, such as solar energy, mechanical vibration, and thermal energy, via solar cell, nanogenerator, and thermoelectric module, respectively, into electrical energy (**Figure 9**a). Then, the obtained electrical energy can be directly stored in the MEESDs, e.g., MBs and MSCs, and can be applied to drive the normal operation of the microelectronic modules, e.g. microscale sensor, small display, and micro-electromechanical systems (Figure 9c), whenever and wherever they are needed. Regarding the MEESDs, MBs usually have high energy density, but limited by power density. MSCs possess high power density, while suffering from low energy density. Therefore, it is advisable to choose individually high-energy MBs or high-power MSCs, or combine them together in terms of the specific application environments of miniaturized electronic systems, working in tight and small spaces in the aerospace, military, precision instruments, biomedical, and other fields. Besides the above applications, the utilization of a flexible self-powered standalone microsystem, capable of realizing all flexible components of energy generator, energy storage, and energy consumption integrated on a small area of flexible substrate, is key for specific and urgent applications in the unpredictable occasions of no external power supply or external electricity-cut environments, e.g., intelligent clothing and healthcare sensors. Nevertheless, there are still several intractable problems standing in the way of these innovations, such as the uniformity of different electronics by microfabrication technique, proper cell encapsulation for stable operation, and suitable design of integrated circuits to well match energy generation, energy storage, and energy consumption devices. Moreover, the connected system should be a highly conductive network with seamless electrical interconnection to reduce the series resistance for minimizing the generation of internal heat and energy loss. To achieve this goal, the advanced technologies of high-resolution photolithography and high-precision printing, including screen printing, inkjet printing, and 3D printing (Figure 9b), hold great potential for one-step scalable fabrication of all components of energy harvester, energy storage, and energy consumption, including different current collectors, various electrode materials, electrolytes, high-conductive interconnects, functional integrated circuits, and even encapsulation for the future self-powered microsystems.

Recently, our group reported a universal and cost-effective screen printing technique for rapid and scalable fabrication of graphene-based planar integrated MSCs (IMSCs), using highly conductive graphene ink with remarkable rheological property.[181] IMSCs with shape compatibility, aesthetic property, excellent flexibility, and outstanding modularization were printed on arbitrary substrates in several seconds. The printed IMSCs were free of external metal current collectors and extra interconnections as well as separators. The capacitance and voltage output were easily tailored through well-defined arrangements of MSCs in series or parallel, depending on the specific requirements of microelectronics. As a proof of

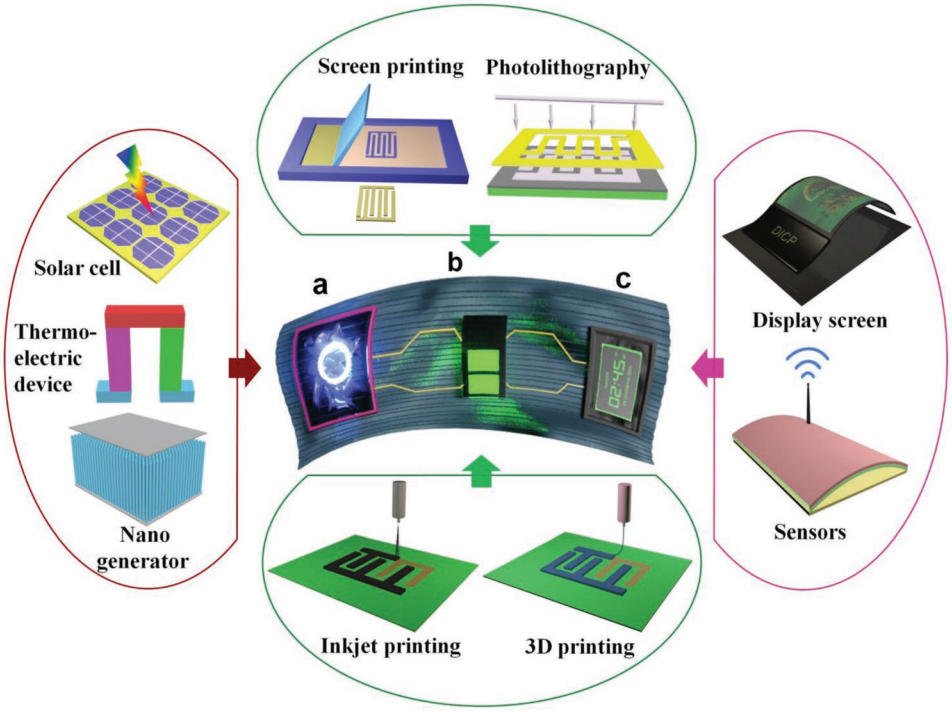

Figure 9. Schematic diagram of flexible self-powered standalone system with energy harvester, energy storage, and energy consumption. a) Energy harvester to convert other energy (solar, mechanical, thermal energy) to electrical energy using solar cell, nanogenerator, and thermoelectric device. b) Scalable manufacture of the monolithic standalone self-powered system using advanced technologies of high-resolution photolithography and printing techniques of screen printing, inkjet printing, and 3D printing. c) Energy consumption of the representative display and sensor.

concept, a tandem pack of IMSCs by integrating 130 MSCs could deliver an ultrahigh voltage over 100 V, demonstrative of numerous opportunities of such IMSCs for miniature high-voltage electronics. Further, an integrated standalone system, composed of tandem asymmetric MSCs based on the interdigital patterns of MnO_2 and polypyrrole, a polyaniline-based gas sensor, and a Si-based solar cell, was constructed on a single paper through screen-printing and electrodeposition strategies.[13] Importantly, the integrated MSCs in this as-fabricated system can efficiently store electrical energy from solar cell, and thus readily drive the gas sensor, displaying a highly sensitive response for NH_3 and HCl. Fan and co-workers[182] demonstrated a printable and wearable self-powered sensing system coupled with inkjet printable MSCs and SnO_2 sensor on a single piece of polyethylene terephthalate (**Figure 10**a–c). MnO_2 based MSCs, SnO_2 microsensors, and integrated circuits were directly printed to construct the monolithic system through relevant printable inks, except for amorphous silicon solar cell and other supporting electronic parts, including light-emitting diode light, voltage regulator, and switches. Such a fully self-powered integrated standalone system mainly consisted of amorphous silicon solar cell, MnO_2 based MSCs, and SnO_2 gas sensor could spontaneously implement sensing function without external charging modules. As a concise functional illustration, self-powered sensor system showed remarkable sensitivity toward ethanol/acetone and the resistance drop resulted from the detection of ethanol/acetone turning on the LED as a warning signal. In addition, Ha and co-workers[14] constructed a highly stretchable strain sensing standalone system based on high-performance all-solid-state MSCs, a strain sensor, and a Si solar cell (Figure 10d–i). By incorporating with the multiple techniques, such as photolithography, e-beam evaporation, and reactive ion etching process, all components on a single deformable polymer substrate were well connected via long serpentine interconnections. When the whole stretchable integrated system in the sun was attached to the wrist under solar irradiation, the arterial pulse could be clearly detected, reflecting the feasibility of wearable functional standalone system. For the optimization of these self-powered standalone systems, higher energy density for MSCs or MBs, higher sensitivity for sensors, and low consumption on interconnection should be further improved. The realization of fully flexible self-power standalone system on a single substrate for practical application has a promising future but there is a long way to go.

6. Conclusions and Perspectives

The MEESDs from MBs to MSCs, serving as microscale standalone energy storage units or complement micropower sources, are undeniably important and in urgent demand for flexible and miniature electronics. Along with accumulating technical readiness level, 2D MEESDs with both in-plane and stacked geometries are gradually moving toward 3D MSCs and MBs with high areal and volumetric energy and power densities. From the development and recent achievements of MBs and MSCs, it is worth noting that the greatest challenge lies

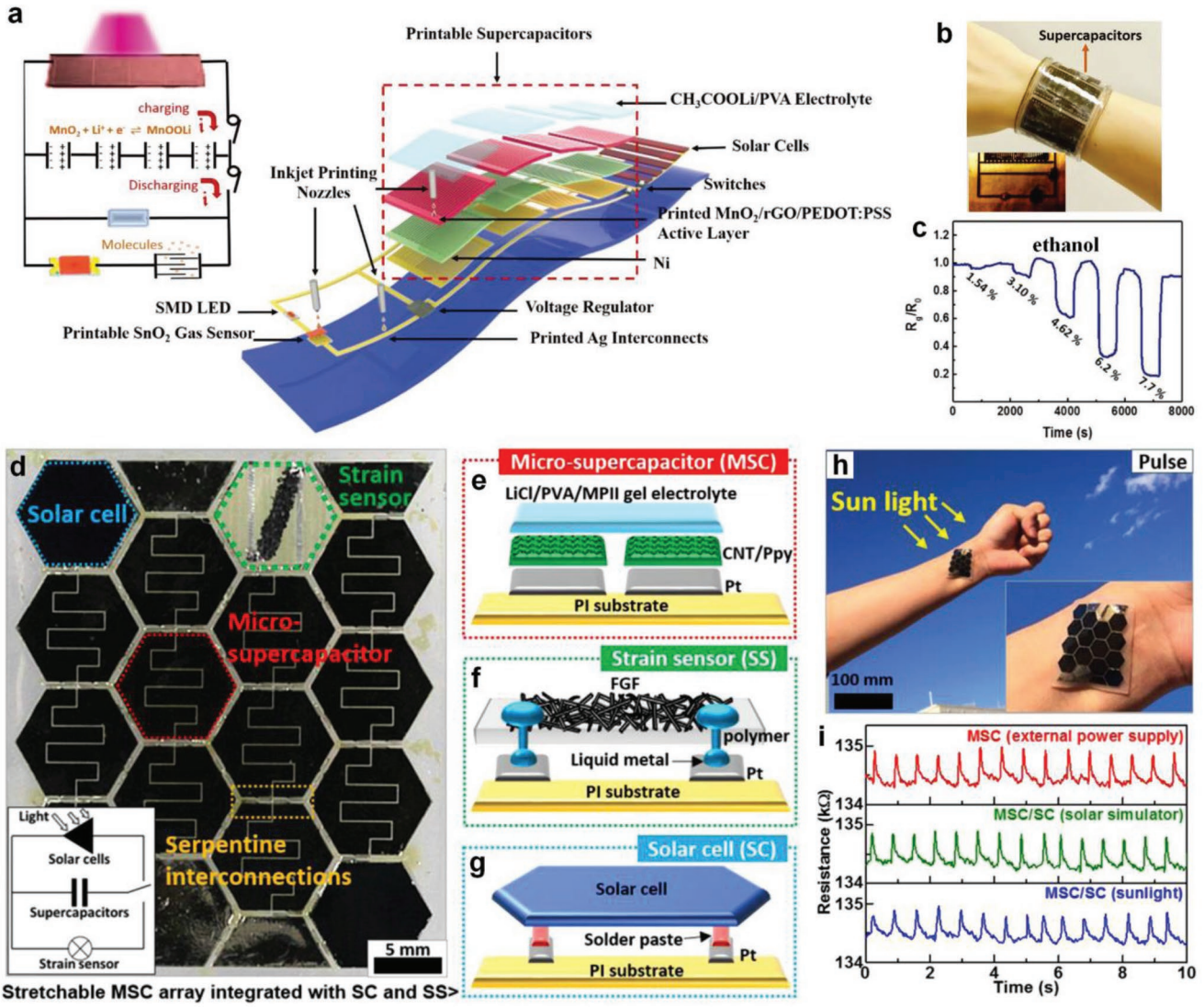

Figure 10. Integration of energy harvesters, energy storage, and energy consumption for flexible standalone system. a) Schematic of monolithically printable integrated self-powered smart sensor system on a plastic substrate. b) Photographs of wearable wristband with a LED as the indicator for gas detection. c) Response and recovery curves of as-printed microsensor toward ethanol at room temperature. Reproduced with permission.[182] Copyright 2018, Wiley-VCH. d) Photograph of the stretchable MSCs array integrated with a solar cell and a strain sensor. e) Schematic of MSCs, f) fragmentized graphene foam-based strain sensor, and g) a solar cell on polyimide substrate. h) Optical image of the integrated system attached on the skin of the wrist. i) Resistance change of the strain sensor driven by the stored energy of the MSCs in response to the pulse signal of the radial artery. d–i) Reproduced with permission.[14] Copyright 2018, Elsevier.

in the overall improvement of both energy density and power density in a confined footprint area/volume of MEESDs with long-term lifespan and multifunctional properties, catering to the various requirements of microelectronics and microsystems. To realize this goal, it is highly recommended to fully consider all device components of MBs and MSCs, including electrode active materials, microelectrode fabrication, selected electrolyte, device configuration, and interfacial contact, listed in details below.

First, the electrochemical performance of MEESDs mainly depends on the inherent properties of electrochemically active materials. To facilitate fast electron transfer and rapid ion diffusion, nanostructured porous electrode materials with high electrical conductivity are expected. Moreover, the electrode materials of particularly pseudocapacitive metal oxide and polymers with small volume change or microelectrode films with tailored pores that can significantly accommodate large volume expansion are highly required to preserve the integrity of microelectrodes without structural fracture and damage during deep charge and discharge process. For example, nanostructured silicon/carbon materials within controllable nanopores, and highly continuous conductive network for electrons and ions are very promising anodes for high-capacity lithium ion MBs,[183,184] while the emerging 2D materials, such as graphene, MXene, MoS_2, have great potential for high-performance MSCs due to their unique open and ultrathin structure, outstanding

flexibility, large accessible surface area, and tunable physical and chemical properties.[185,186] To overcome the shortcomings of individual 2D materials, 2D heterostructures by stacking two different 2D nanosheets or more is considered as an efficient approach to form the synergistic merits. Furthermore, different from conventional active materials, compact thin-film hybrid electrodes combined with hierarchically nanoporous structure and high electrical conductivity also hold tremendous opportunities for constructing MBs and MSCs with high volumetric performance.[121,134,187] Additionally, considerable efforts are still needed to be devoted into the development of new active materials for higher electrochemical and mechanical performance of MBs and MSCs. To understand the structural evolution and ion dynamics of active materials during charge and discharge process, in situ or quasi in situ characterization techniques, such as in situ X-ray diffraction pattern, transmission electron microscopy, electrochemical quartz crystal microbalance (EQCM), and X-ray adsorption spectroscopy, should be considered, all of which are crucial for developing new active materials with high electrochemical performance.

Second, the exploitation of fast, scalable, cost-effective manufacture techniques for fabricating microelectrodes is urgently needed to realize practical implementation of MBs and MSCs. So far, various microfabrication strategies have been developed, including photolithography,[26,53] electrochemical deposition,[112,140] plasma etching,[121,151] photochemistry,[30] mask-assisted filtration,[188] microinjection,[48,60] laser,[44,139] and printing techniques.[189,190] Among them, printing technologies, including 3D printing,[52,102] inkjet printing,[29,96] spray printing,[34,98] and screen printing,[54,124] hold tremendous opportunities for the mass production of MBs and MSCs, which can be directly coupled with the printed electronics, using the same techniques, on the same inflexible, flexible, or stretchable substrate. Importantly, a printable process can be precisely repeated to realize hundreds of micrometers thick microelectrode arrays for improving areal energy density. The key challenges of printable MBs and MSCs include the strategies of preparing a stable active material ink with a proper viscosity for smooth printing, engineering the printable microelectrodes with high electrical conductivity and hierarchical nanostructure, localizing the conformable electrolyte with high ionic conductivity on the project area, and last but not the least, establishing a strong interface of electrode and electrolyte with good wettability for fast ion diffusion. Very importantly, in situ encapsulation that is another key factor for practical application can be also achieved through direct printing of electrolyte resistant airtight polymers. In addition, with the improvement of technological process, high-precision methods like photolithography can manufacture high-resolution microelectrodes and downscale the widths of microelectrodes and interspaces of neighboring electrodes to a nanoscale size, which may be massively beneficial for the mass production of the integrated MBs or MSCs connected in series and in parallel to efficiently boost the voltage and current output in a limited on-chip area.

Third, electrolyte should be rationally selected to well match with MBs and MSCs according to electrode materials, functional properties, and specific purpose. Benefitting from high ionic conductivity, liquid electrolyte-based MBs and MSCs possess superior rate capability and high power density. However, there is a pressing need for cell encapsulation in order to completely prevent electrolyte leakage for safety concerns. Inorganic solid-state electrolytes can form a uniform thin membrane and achieve a stable high voltage up to 5 V, but they present the serious shortcomings of low ionic conductivity at room temperature and poor mechanical performance that is not suitable for flexible MEESDs. Polymer based solid-state electrolyte is made up of the acid, alkali, salt, or ionic liquid and polymers, such as PVA, polyethylene oxide (PEO), and PVDF-HFP. With reasonable optimization, polymer gel electrolyte can achieve higher ionic conductivity than pure liquid electrolyte (e.g., ionic liquid), while some polymers (e.g., PEO) are unstable and prone to decompose at high voltage (e.g., 4 V). In addition, polymer gel electrolyte through the graft of certain functional polymers (e.g., −COOH) is capable of realizing robust stretchability or self-repairability,[191,192] which is crucial for the fabrication of flexible and stretchable MEESDs. One challenge ahead of the functional polymer gel electrolyte lies in maintaining the stable ionic conductivity during deformation. Apart from this, developing redox-based electrolytes would be an effective strategy to boost areal or volumetric capacity of MBs and capacitance of MSCs because of the introduction of redox species that can provide extra charge storage.[193,194] Considering safety issue and biological compatibility, aqueous based electrolytes such as water-in-salt and solvent-in-salt with a large voltage window of up to 4 and 4.5 V, respectively,[91,92] offer dramatic chances to develop high-voltage aqueous and nonaqueous MBs and MSCs for in vivo and wearable microelectronics. Additionally, the functional electrolytes with electrochromic,[195] thermal self-protective,[196] and photoswitching properties[197] have been developed for fast response to external stimuli, while the compatibility between the functional electrolytes and microelectrodes should be seriously considered.

Fourth, in view of the configuration and dimensionality of MBs and MSCs, there remain disparities between electrolyte ions diffusion and microfabrication. 2D stacked MBs and 2D in-plane MSCs have been extensively investigated, from microelectrode materials, solid-state electrolytes to multifunctional properties. Along with the pursuit of high-performance MSCs, asymmetric MSCs and hybrid ion microcapacitors are gradually developed to simultaneously improve the capacitance and voltage. In the case of MSCs, ultrahigh-power MSCs with AC line-filtering performance hold great potential to be seamlessly incorporated with integrated circuit for replacing bulky Al electrolytic capacitors. Differently, there are only a few studies on 3D MBs and 3D MSCs due to the complicated process and requirement of multiple techniques involved, resulting in incomplete usage of the architecture merits of 3D microelectrodes with high-loading active materials. With high active material loading, 3D MBs and 3D MSCs could dramatically enhance areal energy density, which is of great importance for actual applications. But it remains a great challenge to construct electrically conducting, nanoporous, and compact microelectrode arrays with a reliable thickness from tens to hundreds of micrometers. Beyond lithium ion MBs, zinc ion MBs, and symmetric MSCs, developing other high-energy MBs (e.g., lithium–sulfur batteries,[198,199] lithium–air batteries,[200] zinc–air batteries[201]) with miniature architecture and hybrid MSCs (e.g., lithium ion capacitors,[27,202] sodium ion capacitors,[203] and zinc

ion capacitors[204]) may be an effective approach to improve areal or volumetric energy density of MEESDs. As compared with stacked microdevices, in-plane MBs and MSCs possess unique metrics of multidirectional electrolyte ion diffusion for greatly boosting rate capability.[56] However, the investigation and understanding of the ion transfer mechanism for in-plane MBs and MSCs are still at their infancy. Thereby more research works on theoretical simulation and in situ characterization (e.g., Raman spectroscopy, infrared spectroscopy, and EQCM) should be done to optimize the device architectures and sizes for improving the energy and power densities.

Fifth, the dynamics of ion-electron conversion of MBs and MSCs is mainly determined by interfaces, which have a significant effect on rate capability, energy, and power densities. In principle, MBs and MSCs have at least two important interfaces, one between microelectrodes and current collectors, and another between microelectrodes and electrolyte. In general, the compatible and strongly coupled interfaces can substantially reduce the interfacial resistance, facilitate electron transfer between microelectrodes and current collectors, and accelerate the ion diffusion between microelectrodes and electrolyte, thus contributing to high rate capability and low energy loss induced by internal resistance. In particular, the future flexible MBs and MSCs with multifunctionalities of foldability and stretchability are highly required to possess strong interfacial interaction in order to preserve their intimate contact with each other without delamination and fracture when they are subjected to deformation under stress. Usually, the interfaces between microelectrodes and electrolyte can be significantly improved via heteroatomic doping,[205] introducing vacancies[206] and modifying surface[207] of electrodes, which aims to enhance the wettability between them. On the other hand, directly forming bonds,[208] introducing intermediate layers,[209] and direct growth of electrodes[127] on current collectors are useful strategies for producing strongly coupled interfaces between microelectrodes and current collectors. As demonstrated in Si–Li_3PO_4–$LiCoO_2$ MBs, the formation of lithium immobilization layer at the interface between electrode and solid electrolyte has a remarkable influence on the cycling performance.[210] Therefore, more studies should be devoted to the interfacial engineering, including the composition, modification, evolution, and dynamics of the interfaces.

Based on the recent advances and device fabrication development of MEESDs, the future trend of areal and volumetric energy density of these MBs and MSCs can be predicted. Within the next five to ten years, to satisfy the growth of flexible and miniature electronics operating over long periods of time, increasing the volumetric energy density through the continuous research and development of MBs from lithium ion MBs to other high-energy MBs, e.g., lithium–sulfur/air MBs, and high-voltage hybrid MSCs, by a factor of two or more, could be a reliable direction toward dimensionally defined MEESDs as standalone or complementary micropower sources for practical applications. Additionally, a key application for MBs and MSCs is to engineer a self-powered standalone integrated system with smart functions on a single substrate. The major challenges for the realization of such integrated system lie in the lack of one-step, efficient microfabrication method to simultaneously construct the different components with strong compatibility, e.g., energy harvester, energy storage, energy consumption, as well the continuous connection of external circuits and suitable encapsulation for each components. To this end, printing techniques, including inkjet printing, screen printing, and 3D printing, are considered as the all-in-one advanced strategies for the overall design of most possible device components, e.g., microelectrodes, current collectors, electrolyte filling, conductive circuit, and even direct encapsulation. Moreover, the total energy conversion efficiency from energy harvester to energy consumption should be taken into account, which could be improved through the full consideration of the overall system, and the improvement of overall compatibility between various components. It is predicted that the accumulated technical readiness level will highly facilitate the rapid development of the self-powered standalone integrated systems in the near future with various functions (e.g., implantable microdevices and healthcare sensors). Therefore, it is believed that the planar MEESDs of MBs and MSCs are ideal micropower sources for planar integrated circuits and microsystems applications, where a high level of integration, particularly in all-in-one self-powered standalone microsystems, is required.

Acknowledgements

This work was financially supported by the National Natural Science Foundation of China (Grant nos. 51572259 and 51872283), National Key R&D Program of China (Grant nos. 2016YFB0100100 and 2016YFA0200200), Natural Science Foundation of Liaoning Province (Grant no. 20180510038), LiaoNing Revitalization Talents Program (Grant XLYC1807153), DICP (Grant nos. DICP ZZBS201708 and DICP ZZBS201802), DICP&QIBEBT (Grant no. DICP&QIBEBT UN201702), Dalian National Laboratory For Clean Energy (DNL), CAS, DNL Cooperation Fund, CAS (Grant nos. DNL180310 and DNL180308), and Exploratory Research Program of Shaanxi Yanchang Petroleum (Group) CO., LTD & DICP.

Conflict of Interest

The authors declare no conflict of interest.

Keywords

device integration, energy storage, microbatteries, microsupercapacitors, planar devices

Received: January 24, 2019
Revised: April 14, 2019
Published online:

[1] J. A. Rogers, T. Someya, Y. G. Huang, *Science* **2010**, *327*, 1603.
[2] N. A. Kyeremateng, T. Brousse, D. Pech, *Nat. Nanotechnol.* **2017**, *12*, 7.
[3] P. Huang, C. Lethien, S. Pinaud, K. Brousse, R. Laloo, V. Turq, M. Respaud, A. Demortière, B. Daffos, P. L. Taberna, B. Chaudret, Y. Gogotsi, P. Simon, *Science* **2016**, *351*, 691.
[4] A. Sumboja, J. Liu, W. G. Zheng, Y. Zong, H. Zhang, Z. Liu, *Chem. Soc. Rev.* **2018**, *47*, 5919.
[5] P. Zhang, F. Wang, M. Yu, X. Zhuang, X. Feng, *Chem. Soc. Rev.* **2018**, *47*, 7426.

[6] S. W. Pan, J. Ren, X. Fang, H. S. Peng, *Adv. Energy Mater.* **2016**, *6*, 1501867.
[7] M. Beidaghi, Y. Gogotsi, *Energy Environ. Sci.* **2014**, *7*, 867.
[8] J. F. M. Oudenhoven, L. Baggetto, P. H. L. Notten, *Adv. Energy Mater.* **2011**, *1*, 10.
[9] Z. Wen, M. H. Yeh, H. Guo, J. Wang, Y. Zi, W. Xu, J. Deng, L. Zhu, X. Wang, C. Hu, *Sci. Adv.* **2016**, *2*, e1600097.
[10] J. Z. Lee, T. A. Wynn, Y. S. Meng, D. Santhanagopalan, *J. Vis. Exp.* **2018**, *133*, 56259.
[11] A. Ferris, B. Reig, A. Eddarir, J.-F. Pierson, S. Garbarino, D. Guay, D. Pech, *ACS Energy Lett.* **2017**, *2*, 1734.
[12] D. E. Lobo, P. C. Banerjee, C. D. Easton, M. Majumder, *Adv. Energy Mater.* **2015**, *5*, 1500665.
[13] R. Guo, J. Chen, B. Yang, L. Liu, L. Su, B. Shen, X. Yan, *Adv. Funct. Mater.* **2017**, *27*, 1702394.
[14] J. Yun, C. Song, H. Lee, H. Park, Y. R. Jeong, J. W. Kim, S. W. Jin, S. Y. Oh, L. Sun, G. Zi, J. S. Ha, *Nano Energy* **2018**, *49*, 644.
[15] Q. Jiang, C. S. Wu, Z. J. Wang, A. C. Wang, J. H. He, Z. L. Wang, H. N. Alshareef, *Nano Energy* **2018**, *45*, 266.
[16] X. F. Wang, Y. J. Yin, F. Yi, K. R. Dai, S. M. Niu, Y. Z. Han, Y. Zhang, Z. You, *Nano Energy* **2017**, *39*, 429.
[17] L. Y. Yuan, X. Xiao, T. P. Ding, J. W. Zhong, X. H. Zhang, Y. Shen, B. Hu, Y. H. Huang, J. Zhou, Z. L. Wang, *Angew. Chem., Int. Ed.* **2012**, *51*, 4934.
[18] Y. T. Jao, P. K. Yang, C. M. Chiu, Y. J. Lin, S. W. Chen, D. Choi, Z. H. Lin, *Nano Energy* **2018**, *50*, 513.
[19] M. A. P. Mahmud, N. Huda, S. H. Farjana, M. Asadnia, C. Lang, *Adv. Energy Mater.* **2018**, *8*, 1701210.
[20] S. L. Zhai, C. J. Wang, H. E. Karahan, Y. Q. Wang, X. C. Chen, X. Sui, Q. W. Huang, X. Z. Liao, X. Wang, Y. Chen, *Small* **2018**, *14*, 1800582.
[21] X. Fan, J. Chen, J. Yang, P. Bai, Z. L. Li, Z. L. Wang, *ACS Nano* **2015**, *9*, 4236.
[22] F. Yi, L. Lin, S. M. Niu, P. K. Yang, Z. N. Wang, J. Chen, Y. S. Zhou, Y. L. Zi, J. Wang, Q. L. Liao, Y. Zhang, Z. L. Wang, *Adv. Funct. Mater.* **2015**, *25*, 3688.
[23] R. Salot, S. Martin, S. Oukassi, M. Bedjaoui, J. Ubrig, *Appl. Surf. Sci.* **2009**, *256*, S54.
[24] S. Ferrari, M. Loveridge, S. D. Beattie, M. Jahn, R. J. Dashwood, R. Bhagat, *J. Power Sources* **2015**, *286*, 25.
[25] L. X. Liu, Q. H. Weng, X. Y. Lu, X. L. Sun, L. Zhang, O. G. Schmidt, *Small* **2017**, *13*, 1701847.
[26] J. Chmiola, C. Largeot, P. L. Taberna, P. Simon, Y. Gogotsi, *Science* **2010**, *328*, 480.
[27] S. Zheng, J. Ma, Z.-S. Wu, F. Zhou, Y. He, F. Kang, H.-M. Cheng, X. Bao, *Energy Environ. Sci.* **2018**, *11*, 2001.
[28] Z.-S. Wu, X. Feng, H.-M. Cheng, *Natl. Sci. Rev.* **2014**, *1*, 277.
[29] K.-H. Choi, J. Yoo, C. K. Lee, S.-Y. Lee, *Energy Environ. Sci.* **2016**, *9*, 2812.
[30] S. Wang, Z.-S. Wu, S. Zheng, F. Zhou, C. Sun, H.-M. Cheng, X. Bao, *ACS Nano* **2017**, *11*, 4283.
[31] B. L. Ellis, P. Knauth, T. Djenizian, *Adv. Mater.* **2014**, *26*, 3368.
[32] J. Ren, L. Li, C. Chen, X. L. Chen, Z. B. Cai, L. B. Qiu, Y. G. Wang, X. R. Zhu, H. S. Peng, *Adv. Mater.* **2013**, *25*, 1155.
[33] D. S. Yu, K. Goh, H. Wang, L. Wei, W. C. Jiang, Q. Zhang, L. M. Dai, Y. Chen, *Nat. Nanotechnol.* **2014**, *9*, 555.
[34] Z. Liu, Z.-S. Wu, S. Yang, R. Dong, X. Feng, K. Müllen, *Adv. Mater.* **2016**, *28*, 2217.
[35] X. Shi, Z.-S. Wu, J. Qin, S. Zheng, S. Wang, F. Zhou, C. Sun, X. Bao, *Adv. Mater.* **2017**, *29*, 1703034.
[36] J. Meng, H. Guo, C. Niu, Y. Zhao, L. Xu, Q. Li, L. Mai, *Joule* **2017**, *1*, 522.
[37] G. Zhou, F. Li, H.-M. Cheng, *Energy Environ. Sci.* **2014**, *7*, 1307.
[38] J. Mei, T. Liao, L. Kou, Z. Sun, *Adv. Mater.* **2017**, *29*, 1700176.
[39] D. Qi, Y. Liu, Z. Liu, L. Zhang, X. Chen, *Adv. Mater.* **2017**, *29*, 1602802.
[40] F. X. Wang, X. W. Wu, X. H. Yuan, Z. C. Liu, Y. Zhang, L. J. Fu, Y. S. Zhu, Q. M. Zhou, Y. P. Wu, W. Huang, *Chem. Soc. Rev.* **2017**, *46*, 6816.
[41] Prateek, V. K. Thakur, R. K. Gupta, *Chem. Rev.* **2016**, *116*, 4260.
[42] A. Tyagi, K. M. Tripathi, R. K. Gupta, *J. Mater. Chem. A* **2015**, *3*, 22507.
[43] W. Liu, M.-S. Song, B. Kong, Y. Cui, *Adv. Mater.* **2017**, *29*, 1603436.
[44] M. F. El-Kady, R. B. Kaner, *Nat. Commun.* **2013**, *4*, 1475.
[45] W. Gao, N. Singh, L. Song, Z. Liu, A. L. M. Reddy, L. J. Ci, R. Vajtai, Q. Zhang, B. Q. Wei, P. M. Ajayan, *Nat. Nanotechnol.* **2011**, *6*, 496.
[46] S. Zheng, X. Tang, Z.-S. Wu, Y.-Z. Tan, S. Wang, C. Sun, H.-M. Cheng, X. Bao, *ACS Nano* **2017**, *11*, 2171.
[47] M. Nathan, D. Golodnitsky, V. Yufit, E. Strauss, T. Ripenbein, I. Shechtman, S. Menkin, E. Peled, *J. Microelectromech. Syst.* **2005**, *14*, 879.
[48] K. Dokko, J.-i. Sugaya, H. Nakano, T. Yasukawa, T. Matsue, K. Kanamura, *Electrochem. Commun.* **2007**, *9*, 857.
[49] F. Chamran, Y. Yeh, H. S. Min, B. Dunn, C. J. Kim, *J. Microelectromech. Syst.* **2007**, *16*, 844.
[50] H.-S. Min, B. Y. Park, L. Taherabadi, C. Wang, Y. Yeh, R. Zaouk, M. J. Madou, B. Dunn, *J. Power Sources* **2008**, *178*, 795.
[51] M. Koo, K.-I. Park, S. H. Lee, M. Suh, D. Y. Jeon, J. W. Choi, K. Kang, K. J. Lee, *Nano Lett.* **2012**, *12*, 4810.
[52] K. Sun, T.-S. Wei, B. Y. Ahn, J. Y. Seo, S. J. Dillon, J. A. Lewis, *Adv. Mater.* **2013**, *25*, 4539.
[53] H. L. Ning, J. H. Pikul, R. Y. Zhang, X. J. Li, S. Xu, J. J. Wang, J. A. Rogers, W. P. King, P. V. Braun, *Proc. Natl. Acad. Sci. USA* **2015**, *112*, 6573.
[54] R. Kumar, J. Shin, L. Yin, J. M. You, Y. S. Meng, J. Wang, *Adv. Energy Mater.* **2017**, *7*, 1602096.
[55] J. Zhao, K. K. Sonigara, J. Li, J. Zhang, B. Chen, J. Zhang, S. S. Soni, X. Zhou, G. Cui, L. Chen, *Angew. Chem. Int. Ed.* **2017**, *129*, 7979.
[56] S. Zheng, Z.-S. Wu, F. Zhou, X. Wang, J. Ma, C. Liu, Y.-B. He, X. Bao, *Nano Energy* **2018**, *51*, 613.
[57] K. Kanehori, K. Matsumoto, K. Miyauchi, T. Kudo, *Solid State Ionics* **1983**, *9–10*, 1445.
[58] J.-K. Ahn, S.-G. Yoon, *Electrochem. Solid-State Lett.* **2005**, *8*, A75.
[59] S. W. Song, K. C. Lee, H. Y. Park, *J. Power Sources* **2016**, *328*, 311.
[60] K. Yoshima, H. Munakata, K. Kanamura, *J. Power Sources* **2012**, *208*, 404.
[61] J. H. Pikul, H. G. Zhang, J. Cho, P. V. Braun, W. P. King, *Nat. Commun.* **2013**, *4*, 2747.
[62] A. M. Gaikwad, A. M. Zamarayeva, J. Rousseau, H. Chu, I. Derin, D. A. Steingart, *Adv. Mater.* **2012**, *24*, 5071.
[63] J. I. Hur, L. C. Smith, B. Dunn, *Joule* **2018**, *2*, 1187.
[64] M. Letiche, E. Eustache, J. Freixas, A. Demortiere, V. De Andrade, L. Morgenroth, P. Tilmant, F. Vaurette, D. Troadec, P. Roussel, T. Brousse, C. Lethien, *Adv. Energy Mater.* **2017**, *7*, 1601402.
[65] E. Ostreng, K. B. Gandrud, Y. Hu, O. Nilsen, H. Fjellvag, *J. Mater. Chem. A* **2014**, *2*, 15044.
[66] M. E. Donders, W. M. Arnoldbik, H. C. M. Knoops, W. M. M. Kessels, P. H. L. Notten, *J. Electrochem. Soc.* **2013**, *160*, A3066.
[67] K. Tadanaga, A. Yamaguchi, A. Sakuda, A. Hayashi, M. Tatsumisago, A. Duran, M. Aparacio, *Mater. Res. Bull.* **2014**, *53*, 196.
[68] J. Mosa, M. Aparicio, A. Duran, C. Laberty-Robert, C. Sanchez, *J. Mater. Chem. A* **2014**, *2*, 3038.
[69] Y. Wang, J. Roller, R. Maric, *Electrochim. Acta* **2017**, *241*, 510.
[70] M. Hess, E. Lebraud, A. Levasseur, *J. Power Sources* **1997**, *68*, 204.
[71] Y. P. Wu, E. Rahm, R. Holze, *J. Power Sources* **2003**, *114*, 228.

[72] E. Biserni, A. Scarpellini, A. Li Bassi, P. Bruno, Y. Zhou, M. Xie, *Nanotechnology* **2016**, *27*, 245401.
[73] J. L. Chuang YUE, L. LIN, *Front. Mech. Eng.* **2017**, *12*, 459.
[74] A. Lamberti, N. Garino, A. Sacco, S. Bianco, A. Chiodoni, C. Gerbaldi, *Electrochim. Acta* **2015**, *151*, 222.
[75] J. Deng, Z. Lu, I. Belharouak, K. Amine, C. Y. Chung, *J. Power Sources* **2009**, *193*, 816.
[76] M. P. F. Graça, M. A. Valente, M. G. Ferreira da Silva, *J. Non-Cryst. Solids* **2003**, *325*, 267.
[77] T. Ohtomo, A. Hayashi, M. Tatsumisago, Y. Tsuchida, S. Hama, K. Kawamoto, *J. Power Sources* **2013**, *233*, 231.
[78] Y. Inaguma, C. Liquan, M. Itoh, T. Nakamura, T. Uchida, H. Ikuta, M. Wakihara, *Solid State Commun.* **1993**, *86*, 689.
[79] W. Li, M. Wang, Z. H. Li, X. F. Shang, H. Wang, Y. W. Wang, Y. B. Xu, *Russ. J. Electrochem.* **2007**, *43*, 1279.
[80] B. Put, P. M. Vereecken, J. Meersschaut, A. Sepulveda, A. Stesmans, *ACS Appl. Mater. Interfaces* **2016**, *8*, 7060.
[81] Y. Deng, C. Eames, B. Fleutot, R. David, J. N. Chotard, E. Suard, C. Masquelier, M. S. Islam, *ACS Appl. Mater. Interfaces* **2017**, *9*, 7050.
[82] C. Sun, J. Liu, Y. Gong, D. P. Wilkinson, J. Zhang, *Nano Energy* **2017**, *33*, 363.
[83] D. S. Ashby, R. H. DeBlock, C.-H. Lai, C. S. Choi, B. S. Dunn, *Joule* **2017**, *1*, 344.
[84] S.-I. Cho, S.-G. Yoon, *J. Electrochem. Soc.* **2002**, *149*, A1584.
[85] L. Baggetto, R. A. H. Niessen, P. H. L. Notten, *Electrochim. Acta* **2009**, *54*, 5937.
[86] D. Brassard, S. Fourmaux, M. Jean-Jacques, J. C. Kieffer, M. A. E. Khakani, *Appl. Phys. Lett.* **2005**, *87*, 051910.
[87] J. Hong, C. S. Wang, N. J. Dudney, M. J. Lance, *J. Electrochem. Soc.* **2007**, *154*, A805.
[88] Y. H. Rho, K. Kanamura, M. Fujisaki, J.-i. Hamagami, S.-i. Suda, T. Umegaki, *Solid State Ionics* **2002**, *151*, 151.
[89] T. Matsushita, K. Dokko, K. Kanamura, *J. Electrochem. Soc.* **2005**, *152*, A2229.
[90] D. H. Levy, S. F. Nelson, D. Freeman, *J. Display Technol.* **2009**, *5*, 484.
[91] L. Suo, O. Borodin, T. Gao, M. Olguin, J. Ho, X. Fan, C. Luo, C. Wang, K. Xu, *Science* **2015**, *350*, 938.
[92] C. Yang, J. Chen, T. Qing, X. Fan, W. Sun, A. von Cresce, M. S. Ding, O. Borodin, J. Vatamanu, M. A. Schroeder, N. Eidson, C. Wang, K. Xu, *Joule* **2017**, *1*, 122.
[93] H. Nakano, K. Dokko, J.-i. Sugaya, T. Yasukawa, T. Matsue, K. Kanamura, *Electrochem. Commun.* **2007**, *9*, 2013.
[94] M. Kotobuki, Y. Suzuki, H. Munakata, K. Kanamura, Y. Sato, K. Yamamoto, T. Yoshida, *Electrochim. Acta* **2011**, *56*, 1023.
[95] L. Wen, F. Li, H.-M. Cheng, *Adv. Mater.* **2016**, *28*, 4306.
[96] S. Lawes, Q. Sun, A. Lushington, B. W. Xiao, Y. L. Liu, X. L. Sun, *Nano Energy* **2017**, *36*, 313.
[97] Z. Q. Wang, R. Winslow, D. Madan, P. K. Wright, J. W. Evans, M. Keif, X. Y. Rong, *J. Power Sources* **2014**, *268*, 246.
[98] N. Singh, C. Galande, A. Miranda, A. Mathkar, W. Gao, A. L. M. Reddy, A. Vlad, P. M. Ajayan, *Sci. Rep.* **2012**, *2*, 481.
[99] S. Ohta, S. Komagata, J. Seki, T. Saeki, S. Morishita, T. Asaoka, *J. Power Sources* **2013**, *238*, 53.
[100] K. Y. Kang, Y. G. Lee, D. O. Shin, J. C. Kim, K. M. Kim, *Electrochim. Acta* **2014**, *138*, 294.
[101] K. Braam, V. Subramanian, *Adv. Mater.* **2015**, *27*, 689.
[102] K. Fu, Y. Wang, C. Yan, Y. Yao, Y. Chen, J. Dai, S. Lacey, Y. Wang, J. Wan, T. Li, Z. Wang, Y. Xu, L. Hu, *Adv. Mater.* **2016**, *28*, 2587.
[103] B. He, Q. C. Zhang, L. H. Li, J. Sun, P. Man, Z. Y. Zhou, Q. L. Li, J. B. Guo, L. Y. Xie, C. W. Li, X. N. Wang, J. X. Zhao, T. Zhang, Y. G. Yao, *J. Mater. Chem. A* **2018**, *6*, 14594.
[104] C. Wang, L. Taherabadi, G. Jia, M. Madou, Y. Yeh, B. Dunn, *Electrochem. Solid-State Lett.* **2004**, *7*, A435.
[105] Z.-S. Wu, Y.-Z. Tan, S. Zheng, S. Wang, K. Parvez, J. Qin, X. Shi, C. Sun, X. Bao, X. Feng, K. Müllen, *J. Am. Chem. Soc.* **2017**, *139*, 4506.
[106] H. Hu, Z. Pei, C. Ye, *Energy Storage Mater.* **2015**, *1*, 82.
[107] J. Ye, H. Tan, S. Wu, K. Ni, F. Pan, J. Liu, Z. Tao, Y. Qu, H. Ji, P. Simon, Y. Zhu, *Adv. Mater.* **2018**, *30*, 1801384.
[108] C. Zhao, Y. Liu, S. Beirne, J. Razal, J. Chen, *Adv. Mater. Technol.* **2018**, *3*, 1800028.
[109] J. Wang, F. Li, F. Zhu, O. G. Schmidt, *Small Methods* **2018**, *0*, 1800367.
[110] J. H. Sung, S. J. Kim, K. H. Lee, *J. Power Sources* **2003**, *124*, 343.
[111] J.-H. Sung, S.-J. Kim, S.-H. Jeong, E.-H. Kim, K.-H. Lee, *J. Power Sources* **2006**, *162*, 1467.
[112] D. Pech, M. Brunet, H. Durou, P. H. Huang, V. Mochalin, Y. Gogotsi, P. L. Taberna, P. Simon, *Nat. Nanotechnol.* **2010**, *5*, 651.
[113] M. Beidaghi, C. Wang, *Electrochim. Acta* **2011**, *56*, 9508.
[114] Z. S. Wu, K. Parvez, X. L. Feng, K. Müllen, *Nat. Commun.* **2013**, *4*, 2487.
[115] S. Liu, J. Xie, H. Li, Y. Wang, H. Y. Yang, T. Zhu, S. Zhang, G. Cao, X. Zhao, *J. Mater. Chem. A* **2014**, *2*, 18125.
[116] V. G. Rocha, E. García-Tuñón, C. Botas, F. Markoulidis, E. Feilden, E. D'Elia, N. Ni, M. Shaffer, E. Saiz, *ACS Appl. Mater. Interfaces* **2017**, *9*, 37136.
[117] H. Xiao, Z.-S. Wu, F. Zhou, S. Zheng, D. Sui, Y. Chen, X. Bao, *Energy Storage Mater.* **2018**, *13*, 233.
[118] J. H. Lim, D. J. Choi, H.-K. Kim, W. I. Cho, Y. S. Yoon, *J. Electrochem. Soc.* **2001**, *148*, A275.
[119] S. Zheng, W. Lei, J. Qin, Z.-S. Wu, F. Zhou, S. Wang, X. Shi, C. Sun, Y. Chen, X. Bao, *Energy Storage Mater.* **2018**, *10*, 24.
[120] Y.-Y. Peng, B. Akuzum, N. Kurra, M.-Q. Zhao, M. Alhabeb, B. Anasori, E. C. Kumbur, H. N. Alshareef, M.-D. Ger, Y. Gogotsi, *Energy Environ. Sci.* **2016**, *9*, 2847.
[121] Z. S. Wu, K. Parvez, S. Li, S. Yang, Z. Y. Liu, S. H. Liu, X. L. Feng, K. Müllen, *Adv. Mater.* **2015**, *27*, 4054.
[122] F. Zhou, H. Huang, C. Xiao, S. Zheng, X. Shi, J. Qin, Q. Fu, X. Bao, X. Feng, K. Müllen, Z.-S. Wu, *J. Am. Chem. Soc.* **2018**, *140*, 8198.
[123] M. F. El-Kady, M. Ihns, M. Li, J. Y. Hwang, M. F. Mousavi, L. Chaney, A. T. Lech, R. B. Kaner, *Proc. Natl. Acad. Sci. USA* **2015**, *112*, 4233.
[124] S. Xu, Y. Dall'Agnese, G. Wei, C. Zhang, Y. Gogotsi, W. Han, *Nano Energy* **2018**, *50*, 479.
[125] P. Zhang, Y. Li, G. Wang, F. Wang, S. Yang, F. Zhu, X. Zhuang, O. G. Schmidt, X. Feng, *Adv. Mater.* **2019**, *31*, 1806005.
[126] Y. Yue, Z. Yang, N. Liu, W. Liu, H. Zhang, Y. Ma, C. Yang, J. Su, L. Li, F. Long, Z. Zou, Y. Gao, *ACS Nano* **2016**, *10*, 11249.
[127] J. Lin, C. Zhang, Z. Yan, Y. Zhu, Z. Peng, R. H. Hauge, D. Natelson, J. M. Tour, *Nano Lett.* **2013**, *13*, 72.
[128] E. Eustache, C. Douard, A. Demortière, V. D. Andrade, M. Brachet, J. L. Bideau, T. Brousse, C. Lethien, *Adv. Mater. Technol.* **2017**, *2*, 1700126.
[129] Y. S. Yoon, W. I. Cho, J. H. Lim, D. J. Choi, *J. Power Sources* **2001**, *101*, 126.
[130] H.-K. Kim, S.-H. Cho, Y.-W. Ok, T.-Y. Seong, Y. S. Yoon, *J. Vac. Sci. Technol., B: Microelectron. Nanometer Struct.–Process., Meas., Phenom.* **2003**, *21*, 949.
[131] M. R. Karim, K. Hatakeyama, T. Matsui, H. Takehira, T. Taniguchi, M. Koinuma, Y. Matsumoto, T. Akutagawa, T. Nakamura, S.-i. Noro, T. Yamada, H. Kitagawa, S. Hayami, *J. Am. Chem. Soc.* **2013**, *135*, 8097.
[132] S. Qin, D. Liu, G. Wang, D. Portehault, C. J. Garvey, Y. Gogotsi, W. Lei, Y. Chen, *J. Am. Chem. Soc.* **2017**, *139*, 6314.
[133] J.-J. Shao, K. Raidongia, A. R. Koltonow, J. Huang, *Nat. Commun.* **2015**, *6*, 7602.
[134] X. Yang, C. Cheng, Y. Wang, L. Qiu, D. Li, *Science* **2013**, *341*, 534.

[135] J. Yan, C. E. Ren, K. Maleski, C. B. Hatter, B. Anasori, P. Urbankowski, A. Sarycheva, Y. Gogotsi, *Adv. Funct. Mater.* **2017**, *27*, 1701264.
[136] J.-H. Sung, S.-J. Kim, K.-H. Lee, *J. Power Sources* **2004**, *133*, 312.
[137] T. M. Dinh, K. Armstrong, D. Guay, D. Pech, *J. Mater. Chem. A* **2014**, *2*, 7170.
[138] Z.-S. Wu, K. Parvez, X. Feng, K. Müllen, *J. Mater. Chem. A* **2014**, *2*, 8288.
[139] J. Lin, Z. Peng, Y. Liu, F. Ruiz-Zepeda, R. Ye, E. L. G. Samuel, M. J. Yacaman, B. I. Yakobson, J. M. Tour, *Nat. Commun.* **2014**, *5*, 5714.
[140] L. Li, J. Zhang, Z. Peng, Y. Li, C. Gao, Y. Ji, R. Ye, N. D. Kim, Q. Zhong, Y. Yang, H. Fei, G. Ruan, J. M. Tour, *Adv. Mater.* **2016**, *28*, 838.
[141] D. Pech, M. Brunet, P.-L. Taberna, P. Simon, N. Fabre, F. Mesnilgrente, V. Conédéra, H. Durou, *J. Power Sources* **2010**, *195*, 1266.
[142] Z.-S. Wu, K. Parvez, A. Winter, H. Vieker, X. Liu, S. Han, A. Turchanin, X. Feng, K. Müllen, *Adv. Mater.* **2014**, *26*, 4552.
[143] Z. Xiong, X. Yun, L. Qiu, Y. Sun, B. Tang, Z. He, J. Xiao, D. Chung, T. W. Ng, H. Yan, R. Zhang, X. Wang, D. Li, *Adv. Mater.* **2019**, *31*, 1804434.
[144] N. Kurra, B. Ahmed, Y. Gogotsi, H. N. Alshareef, *Adv. Energy Mater.* **2016**, *6*, 1601372.
[145] H. Li, Y. Hou, F. Wang, M. R. Lohe, X. Zhuang, L. Niu, X. Feng, *Adv. Energy Mater.* **2017**, *7*, 1601847.
[146] C. Zhang, M. P. Kremer, A. Seral-Ascaso, S.-H. Park, N. McEvoy, B. Anasori, Y. Gogotsi, V. Nicolosi, *Adv. Funct. Mater.* **2018**, *28*, 1705506.
[147] W. Yang, L. He, X. C. Tian, M. Y. Yan, H. Yuan, X. B. Liao, J. S. Meng, Z. M. Hao, L. Q. Mai, *Small* **2017**, *13*, 1700639.
[148] J. Li, Q. Shi, Y. Shao, C. Hou, Y. Li, Q. Zhang, H. Wang, *Energy Storage Mater.* **2019**, *16*, 212.
[149] T. M. Dinh, A. Achour, S. Vizireanu, G. Dinescu, L. Nistor, K. Armstrong, D. Guay, D. Pech, *Nano Energy* **2014**, *10*, 288.
[150] Y.-Q. Li, X.-M. Shi, X.-Y. Lang, Z. Wen, J.-C. Li, Q. Jiang, *Adv. Funct. Mater.* **2016**, *26*, 1830.
[151] Z.-S. Wu, Y. Zheng, S. Zheng, S. Wang, C. Sun, K. Parvez, T. Ikeda, X. Bao, K. Müllen, X. Feng, *Adv. Mater.* **2017**, *29*, 1602960.
[152] N. Kurra, Q. Jiang, A. Syed, C. Xia, H. N. Alshareef, *ACS Appl. Mater. Interfaces* **2016**, *8*, 12748.
[153] J. J. Yoo, K. Balakrishnan, J. Huang, V. Meunier, B. G. Sumpter, A. Srivastava, M. Conway, A. L. Mohana Reddy, J. Yu, R. Vajtai, P. M. Ajayan, *Nano Lett.* **2011**, *11*, 1423.
[154] V. Augustyn, Y. Gogotsi, *Joule* **2017**, *1*, 443.
[155] Y. Han, Y. Ge, Y. F. Chao, C. Y. Wang, G. G. Wallace, *J. Energy Chem.* **2018**, *27*, 57.
[156] M. R. Lukatskaya, O. Mashtalir, C. E. Ren, Y. Dall'Agnese, P. Rozier, P. L. Taberna, M. Naguib, P. Simon, M. W. Barsoum, Y. Gogotsi, *Science* **2013**, *341*, 1502.
[157] M. Ghidiu, M. R. Lukatskaya, M.-Q. Zhao, Y. Gogotsi, M. W. Barsoum, *Nature* **2014**, *516*, 78.
[158] M. R. Lukatskaya, S. Kota, Z. Lin, M.-Q. Zhao, N. Shpigel, M. D. Levi, J. Halim, P.-L. Taberna, M. W. Barsoum, P. Simon, Y. Gogotsi, *Nat. Energy* **2017**, *2*, 17105.
[159] C. Zhang, B. Anasori, A. Seral-Ascaso, S.-H. Park, N. McEvoy, A. Shmeliov, G. S. Duesberg, J. N. Coleman, Y. Gogotsi, V. Nicolosi, *Adv. Mater.* **2017**, *29*, 1702678.
[160] S. Zheng, C. Zhang, F. Zhou, Y. Dong, X. Shi, V. Nicolosi, Z.-S. Wu, X. Bao, *J. Mater. Chem. A* **2019**, *7*, 9478.
[161] M. F. El-Kady, Y. Shao, R. B. Kaner, *Nat. Rev. Mater.* **2016**, *1*, 16033.
[162] M. Ye, Z. Zhang, Y. Zhao, L. Qu, *Joule* **2018**, *2*, 245.
[163] K. N. Chen, Q. R. Wang, Z. Q. Niu, J. Chen, *J. Energy Chem.* **2018**, *27*, 12.
[164] M. F. El-Kady, V. Strong, S. Dubin, R. B. Kaner, *Science* **2012**, *335*, 1326.
[165] M. Zhang, S. Makino, D. Mochizuki, W. Sugimoto, *J. Power Sources* **2018**, *396*, 498.
[166] M. Watanabe, M. L. Thomas, S. Zhang, K. Ueno, T. Yasuda, K. Dokko, *Chem. Rev.* **2017**, *117*, 7190.
[167] N. Jabeen, A. Hussain, Q. Xia, S. Sun, J. Zhu, H. Xia, *Adv. Mater.* **2017**, *29*, 1700804.
[168] S. Zheng, Z.-S. Wu, S. Wang, H. Xiao, F. Zhou, C. Sun, X. Bao, H.-M. Cheng, *Energy Storage Mater.* **2017**, *6*, 70.
[169] K. Shen, J. Ding, S. Yang, *Adv. Energy Mater.* **2018**, *8*, 1800408.
[170] Y. He, P. Zhang, M. Wang, F. Wang, D. Tan, Y. Li, X. Zhuang, F. Zhang, X. Feng, *Mater. Horiz.* **2019**, *6*, 1041.
[171] G. Sun, H. Yang, G. Zhang, J. Gao, X. Jin, Y. Zhao, L. Jiang, L. Qu, *Energy Environ. Sci.* **2018**, *11*, 3367.
[172] Z.-S. Wu, Z. Liu, K. Parvez, X. Feng, K. Müllen, *Adv. Mater.* **2015**, *27*, 3669.
[173] M. Zhang, Q. Q. Zhou, J. Chen, X. W. Yu, L. Huang, Y. R. Li, C. Li, G. Q. Shi, *Energy Environ. Sci.* **2016**, *9*, 2005.
[174] Y. Jiang, Z. Xu, T. Huang, Y. Liu, F. Guo, J. Xi, W. Gao, C. Gao, *Adv. Funct. Mater.* **2018**, *28*, 1707024.
[175] X. Pu, M. Liu, L. Li, S. Han, X. Li, C. Jiang, C. Du, J. Luo, W. Hu, Z. L. Wang, *Adv. Energy Mater.* **2016**, *6*, 1601254.
[176] X. S. Zhang, M. D. Han, B. Kim, J. F. Bao, J. Brugger, H. X. Zhang, *Nano Energy* **2018**, *47*, 410.
[177] F. Wu, P. Yu, L. Q. Mao, *Chem. Soc. Rev.* **2017**, *46*, 2692.
[178] B. Wang, C. Liu, Y. Xiao, J. Zhong, W. Li, Y. Cheng, B. Hu, L. Huang, J. Zhou, *Nano Energy* **2017**, *32*, 42.
[179] Z. Zhang, X. Chen, P. Chen, G. Guan, L. Qiu, H. Lin, Z. Yang, W. Bai, Y. Luo, H. Peng, *Adv. Mater.* **2014**, *26*, 466.
[180] J. Cai, C. Lv, A. Watanabe, *Nano Energy* **2016**, *30*, 790.
[181] X. Shi, S. Pei, F. Zhou, W. Ren, H.-M. Cheng, Z.-S. Wu, X. Bao, *Energy Environ. Sci.* **2019**, *12*, 1534.
[182] Y. Lin, J. Chen, M. M. Tavakoli, Y. Gao, Y. Zhu, D. Zhang, M. Kam, Z. He, Z. Fan, *Adv. Mater.* **2019**, *31*, 1804285.
[183] M. Ko, S. Chae, J. Ma, N. Kim, H. W. Lee, Y. Cui, J. Cho, *Nat. Energy* **2016**, *1*, 16113.
[184] S. Chae, M. Ko, K. Kim, K. Ahn, J. Cho, *Joule* **2017**, *1*, 47.
[185] B. Mendoza-Sanchez, Y. Gogotsi, *Adv. Mater.* **2016**, *28*, 6104.
[186] M. Acerce, D. Voiry, M. Chhowalla, *Nat. Nanotechnol.* **2015**, *10*, 313.
[187] Z. Chen, J. W. F. To, C. Wang, Z. Lu, N. Liu, A. Chortos, L. Pan, F. Wei, Y. Cui, Z. Bao, *Adv. Energy Mater.* **2014**, *4*, 1400207.
[188] H. Xiao, Z.-S. Wu, L. Chen, F. Zhou, S. Zheng, W. Ren, H.-M. Cheng, X. Bao, *ACS Nano* **2017**, *11*, 7284.
[189] F. Zhang, M. Wei, V. V. Viswanathan, B. Swart, Y. Y. Shao, G. Wu, C. Zhou, *Nano Energy* **2017**, *40*, 418.
[190] K. H. Choi, D. B. Ahn, S. Y. Lee, *ACS Energy Lett.* **2018**, *3*, 220.
[191] Y. Huang, M. Zhong, Y. Huang, M. Zhu, Z. Pei, Z. Wang, Q. Xue, X. Xie, C. Zhi, *Nat. Commun.* **2015**, *6*, 10310.
[192] Y. Z. Guo, X. Zhou, Q. Q. Tang, H. Bao, G. C. Wang, P. Saha, *J. Mater. Chem. A* **2016**, *4*, 8769.
[193] J. Kim, J. H. Kim, K. Ariga, *Joule* **2017**, *1*, 739.
[194] S. E. Chun, B. Evanko, X. F. Wang, D. Vonlanthen, X. L. Ji, G. D. Stucky, S. W. Boettcher, *Nat. Commun.* **2015**, *6*, 7818.
[195] P. Zhang, F. Zhu, F. Wang, J. Wang, R. Dong, X. Zhuang, O. G. Schmidt, X. Feng, *Adv. Mater.* **2017**, *29*, 1604491.
[196] P. Zhang, J. Wang, W. Sheng, F. Wang, J. Zhang, F. Zhu, X. Zhuang, R. Jordan, O. G. Schmidt, X. Feng, *Energy Environ. Sci.* **2018**, *11*, 1717.
[197] Z. Liu, H. I. Wang, A. Narita, Q. Chen, Z. Mics, D. Turchinovich, M. Kläui, M. Bonn, K. Müllen, *J. Am. Chem. Soc.* **2017**, *139*, 9443.
[198] X. L. Ji, K. T. Lee, L. F. Nazar, *Nat. Mater.* **2009**, *8*, 500.

[199] Z. W. Seh, Y. M. Sun, Q. F. Zhang, Y. Cui, *Chem. Soc. Rev.* **2016**, *45*, 5605.
[200] H. G. Jung, J. Hassoun, J. B. Park, Y. K. Sun, B. Scrosati, *Nat. Chem.* **2012**, *4*, 579.
[201] Y. G. Li, H. J. Dai, *Chem. Soc. Rev.* **2014**, *43*, 5257.
[202] Y. Ma, H. Chang, M. Zhang, Y. Chen, *Adv. Mater.* **2015**, *27*, 5296.
[203] J. Ding, H. Wang, Z. Li, K. Cui, D. Karpuzov, X. Tan, A. Kohandehghan, D. Mitlin, *Energy Environ. Sci.* **2015**, *8*, 941.
[204] H. Wang, M. Wang, Y. Tang, *Energy Storage Mater.* **2018**, *13*, 1.
[205] Z. S. Wu, W. C. Ren, L. Xu, F. Li, H. M. Cheng, *ACS Nano* **2011**, *5*, 5463.
[206] Y. Zhu, G. H. Yu, *Chem* **2018**, *4*, 1486.
[207] K. X. Wang, X. H. Li, J. S. Chen, *Adv. Mater.* **2015**, *27*, 527.
[208] S. Zheng, Z. Li, Z.-S. Wu, Y. Dong, F. Zhou, S. Wang, Q. Fu, C. Sun, L. Guo, X. Bao, *ACS Nano* **2017**, *11*, 4009.
[209] M. Wang, M. Tang, S. Chen, H. Ci, K. Wang, L. Shi, L. Lin, H. Ren, J. Shan, P. Gao, Z. Liu, H. Peng, *Adv. Mater.* **2017**, *29*, 1703882.
[210] C. Chen, J. F. M. Oudenhoven, D. L. Danilov, E. Vezhlev, L. Gao, N. Li, F. M. Mulder, R.-A. Eichel, P. H. L. Notten, *Adv. Energy Mater.* **2018**, *8*, 1801430.

